

CONFIRMATION OF A CORRELATION BETWEEN THE X-RAY LUMINOSITY AND SPECTRAL SLOPE OF AGNS IN THE CHANDRA DEEP FIELDS.

C. SAEZ¹, G. CHARTAS¹, W. N. BRANDT¹, B. D. LEHMER², F. E. BAUER³, X. DAI⁴, AND G. P. GARMIRE¹

Draft version November 11, 2018

ABSTRACT

We present results from a statistical analysis of 173 bright radio-quiet AGNs selected from the *Chandra* Deep Field-North and *Chandra* Deep Field-South surveys (hereafter, CDFs) in the redshift range of $0.1 \lesssim z \lesssim 4$. We find that the X-ray power-law photon index (Γ) of radio-quiet AGNs is correlated with their 2–10 keV rest-frame X-ray luminosity (L_X) at the $> 99.5\%$ confidence level in two redshift bins, $0.3 \lesssim z \lesssim 0.96$, and $1.5 \lesssim z \lesssim 3.3$ and is slightly less significant in the redshift bin $0.96 \lesssim z \lesssim 1.5$. The X-ray spectral slope steepens as the X-ray luminosity increases for AGNs in the luminosity range 10^{42} to 10^{45} erg s⁻¹. Combining our results from the CDFs with those from previous studies in the redshift range $1.5 \lesssim z \lesssim 3.3$, we find that the $\Gamma - L_X$ correlation has a null-hypothesis probability of 1.6×10^{-9} . We investigate the redshift evolution of the correlation between the power-law photon index and the hard X-ray luminosity and find that the slope and offset of a linear fit to the correlation change significantly (at the $> 99.9\%$ confidence level) between redshift bins of $0.3 \lesssim z \lesssim 0.96$ and $1.5 \lesssim z \lesssim 3.3$. We explore physical scenarios explaining the origin of this correlation and its possible evolution with redshift in the context of steady corona models focusing on its dependency on variations of the properties of the hot corona with redshift.

Subject headings: cosmology: observations — galaxies: active — galaxies: statistics — X-rays: galaxies

1. INTRODUCTION

It is important to extend the study of quasars to high redshifts in order to understand their evolution and environments. A relevant conclusion from modern studies is that the quasar luminosity function evolves positively with redshift, having a comoving space density strongly peaked at $z \approx 2$ (e.g., Schmidt 1968; Boyle et al. 1987; Warren et al. 1994). More recent findings suggest that the evolution of the space density of AGNs is strongly dependent on X-ray luminosity (L_X), with the peak space density of AGNs moving to higher redshifts for more luminous AGNs (e.g., Ueda et al. 2003; Hasinger et al. 2005).

The X-ray band probes the innermost region of the central engines of AGNs. The study of AGNs in the X-ray band provides important insights about their central engines and the evolution of the AGN luminosity function. In most AGNs, the observed X-ray continuum can be modeled using a power-law of the form $N(E) = N_0(E/E_0)^{-\Gamma}$, where Γ is the photon index. This power-law is attenuated by material in our Galaxy as well as material intrinsic to the host galaxy. Several recent studies have centered on estimating the distribution of intrinsic column densities (N_H) and the fraction of AGNs having $N_H \gtrsim 10^{22}$ cm⁻². Recent theoretical studies of AGNs (e.g., Hopkins et al. 2005) suggest that the distribution of N_H is luminosity dependent; this is supported observationally with the detection of an anti-correlation between the obscuration frac-

tion and luminosity (e.g., Steffen et al. 2003; Ueda et al. 2003; La Franca et al. 2005; Akylas et al. 2006). We note, however, recent work by Dwelly & Page (2006) reporting that the obscuration fraction may be independent of luminosity. The dependence of the obscuration fraction on redshift is a controversial issue. Some authors detect an increase of the obscuration fraction with redshift (e.g., La Franca et al. 2005; Treister & Urry 2006; Tozzi et al. 2006), while others do not find any evidence for evolution (e.g., Ueda et al. 2003; Akylas et al. 2006; Dwelly & Page 2006).

A recent mini-survey of relatively high-redshift ($1.5 < z < 4$) gravitationally lensed radio-quiet quasars (RQQs) observed with *Chandra* and *XMM-Newton* (Dai et al. 2004) indicated a possible correlation between the X-ray power-law photon index and X-ray luminosity. This correlation, characterized by an increase of Γ with L_X , was found for RQQs with 2–10 keV luminosities in the range 10^{43} to 10^{45} erg s⁻¹. Such a correlation is not found in nearby $z \lesssim 0.1$ quasars (e.g., George et al. 2000). Several studies to date of high-redshift quasars do not have large enough sample sizes in the 2–10 keV luminosity range 10^{43} to 10^{45} erg s⁻¹ to place any significant constraints on a possible $\Gamma - L_X$ correlation (e.g., Reeves & Turner 2000; Page et al. 2005).

One of the concerns with the Dai et al. (2004) analysis was that the limited number of quasars in the sample, combined with the poor signal-to-noise ratio (S/N) available for several of the observations and the relatively large fraction of BAL quasars, may have led to problematic systematic effects. The number of available lensed radio-quiet quasars used by Dai et al. (2004) was limited to a total of 25 sources, of which the brightest 11 had X-ray observations. In order to increase the size of the high-redshift radio-quiet quasar sample, we have compiled a sample of 173 high-redshift AGNs with moderate-to-

¹ Astronomy and Astrophysics Department, Pennsylvania State University, University Park, PA 16802, USA

² Department of Physics, University of Durham, South Road, Durham, DH1 3LE, UK

³ Columbia Astrophysics Laboratory, Columbia University, New York, NY 10027, USA

⁴ Department of Astronomy, The Ohio State University, Columbus, OH 43210, USA

high S/N spectra available from the *Chandra* Deep-Field-North and *Chandra* Deep-Field-South surveys (CDF-N and CDF-S, respectively; jointly CDFs; Giacconi et al. 2002; Alexander et al. 2003).

The main scientific goal of this work is to constrain better the $\Gamma - L_X$ correlation found by Dai et al. (2004). The significant increase in sample size allows us to place tighter constraints on the significance of the correlation. We also test the correlation in narrower redshift bands which will allow us to determine the epoch by which possible changes in the average emission properties of AGNs occurred. Currently, the two deepest X-ray surveys are the CDF-N and CDF-S with ≈ 2 Ms and ≈ 1 Ms exposures, respectively. Both surveys cover ≈ 300 arcmin² areas and target different regions of the sky characterized by low Galactic column densities and an absence of bright stars (Giacconi et al. 2002; Alexander et al. 2003). The CDFs pointings have sufficient sensitivity to detect the X-ray emission from AGNs with moderate luminosities ($L_X \approx 10^{43} - 10^{44}$ erg s⁻¹) out to $z \approx 2 - 6$.

Radio-quiet AGNs (RQ AGNs) correspond to the majority of active galaxies ($\sim 90\%$) that contain a central active nucleus and show several differences in their spectral properties compared to radio-loud AGNs. Radio-loud AGNs have powerful sub-parsec jet-linked X-ray synchrotron self-Compton (SSC) emission, which introduces an additional component to their spectra. As a consequence RQ AGNs are observed to have, on average, steeper X-ray power-laws than radio-loud AGNs (e.g., Reeves et al. 1997). We therefore have chosen to exclude radio-loud AGNs from this study. Throughout this paper we adopt a flat Λ -dominated universe with $H_0 = 70$ km s⁻¹Mpc⁻¹, $\Omega_\Lambda = 0.7$, and $\Omega_M = 0.3$. The *Chandra* data were reduced using the CIAO version 3.3 software tools provided by the *Chandra* X-ray Center (CXC), and the spectral analysis was performed using XSPEC version 12.

2. SAMPLE SELECTION

Our sources were selected from the CDFs, currently the two deepest X-ray surveys. The on-axis sensitivity limits for the CDF-N are $\approx 2.5 \times 10^{-17}$ erg cm⁻² s⁻¹ (0.5–2.0 keV) and $\approx 1.4 \times 10^{-16}$ erg cm⁻² s⁻¹ (2–8 keV). These limits are around two times more sensitive than those for the CDF-S (Giacconi et al. 2002; Alexander et al. 2003). The CDFs are 50–250 times more sensitive than previous X-ray surveys, detecting ≈ 900 point sources, of which ≈ 600 are AGNs and galaxies with measured redshifts (Giacconi et al. 2002; Alexander et al. 2003; Barger et al. 2003; Zheng et al. 2004).

Spectroscopic and photometric redshifts were gathered from the literature (Croom et al. 2001; Barger et al. 2003; Steidel et al. 2003; Cowie et al. 2004; Mobasher et al. 2004; Szokoly et al. 2004; Wirth et al. 2004; Wolf et al. 2004; Zheng et al. 2004; Alexander et al. 2005; Colbert et al. 2005; Le Fèvre et al. 2005; Vanzella et al. 2006) and vetted to remove redshifts which did not appear to belong to the most-likely optical counterpart to each X-ray source. The latter was assessed by comparing the optical and X-ray images, which were aligned to between $0''.12 - 0''.25$; this notably affected the redshifts from Zheng et al. (2004), where 47 ($\approx 14\%$) of the redshifts were rejected

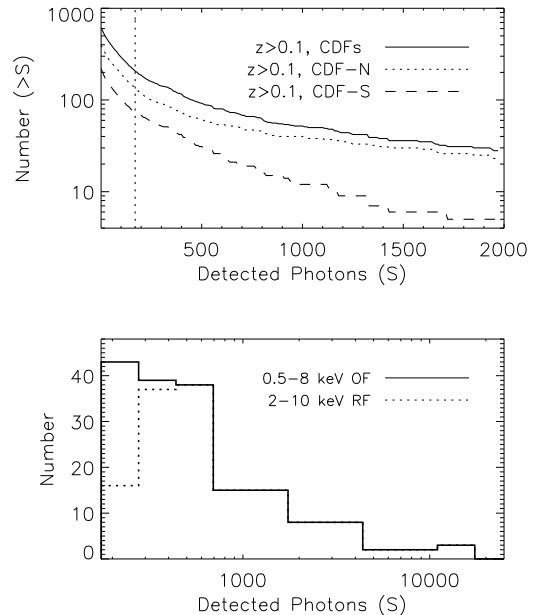


FIG. 1.— (upper panel) Number of sources with more than S photons (0.5–8 keV observed-frame) versus S . The thick line corresponds to all CDFs sources with measured redshifts of $z > 0.1$. The dotted line shows sources of the CDF-N survey with $z \gtrsim 0.1$, and the dashed line shows sources of the CDF-S survey with $z \gtrsim 0.1$. The vertical dotted line corresponds to $S=170$. Note that the sample used to generate this figure contains AGNs (both RQ and radio-loud AGNs), normal galaxies and starburst galaxies. (lower panel) Number of radio-quiet AGNs with $z \gtrsim 0.1$ vs. the number of photons (S ; 0.5–8 keV) in their spectra. The solid line represents sources with fits performed in the 0.5–8 keV observed-frame band and the dotted line represents sources with fits performed in the 2–10 keV rest-frame band.

for being associated with an unlikely optical counterpart. For the ~ 40 faint sources still lacking redshift estimates, we used the BPZ code (Bayesian photometric redshift estimation; Benitez 2000) and available photometry (Arnouts et al. 2001; Barger et al. 2003; Giavalisco et al. 2004) to estimate crude redshifts.

The selection criteria for our sample of RQ AGNs are (1) that the sources are radio-quiet (see below), (2) that the redshifts of the sources are greater than 0.1, and (3) that the total number of photons in the full band (0.5–8 keV) is greater than ~ 170 counts ($S \gtrsim 170$) resulting in moderate-to-high S/N spectra. The selection of a cut-off at ~ 170 counts allows an accurate estimate of the photon index, which is not possible for fainter sources (Tozzi et al. 2006). Based on the condition that $S \gtrsim 170$, the on-axis flux limits of our sample in the full band (0.5–8 keV) in the CDF-N and CDF-S surveys are $\approx 1 \times 10^{-15}$ erg cm⁻² s⁻¹ and $\approx 2 \times 10^{-15}$ erg cm⁻² s⁻¹, respectively.

In Figure 1 (upper panel), we show the cumulative distribution for number of X-ray sources having more than S counts (0.5–8 keV) for the CDF-N and CDF-S. The CDFs contain 205 sources with more than 170 counts at $z > 0.1$. Most of these sources are AGNs; however, in the low-redshift regime of our sample $0.1 \lesssim z \lesssim 1.0$ we expect only a small fraction of starburst and “normal” galaxies (Brandt & Hasinger 2005). Following the classification scheme discussed in §4.1.1 of Bauer et al. (2004a), we found two starburst galaxies and one “nor-

mal” galaxy, which we remove leaving 202 AGNs in our sample.

Radio-loud AGNs were classified based on a radio-loudness parameter $R \gtrsim 10$ ($R = f_{5\text{GHz}}/f_B$). To find these sources, we matched the X-ray positions with radio sources using a matching radius of 2 arcsec. The flux-density at 5 GHz was obtained from the flux-density at 1.4 GHz assuming a power law radio spectrum ($f_\nu \propto \nu^{-\alpha_r}$), where $\alpha_r = 0.8$ is a characteristic radio spectral index of synchrotron radiation⁵.

The flux in the B filter was obtained from Barger et al. (2003) for the CDF-N sources and from public-domain tables of the GOODS and COMBO-17 surveys for the CDF-S sources. When searching the radio catalogs⁶ provided by Richards (2000) for the CDF-N and Afonso et al. (2006) for the CDF-S, we find that 29 ($\sim 14\%$) out of the 202 X-ray detected AGNs were radio-loud. This leaves 173 RQ AGNs which we use for our analysis out of which 111 have spectroscopic redshifts.

3. SPECTRAL EXTRACTION

The X-ray spectra of the sources of the CDFs analyzed in our study were extracted using the software routine ACIS_EXTRACT v3.94 (hereafter AE; Townsley et al. 2003; Broos et al. 2005), included in the Tools for ACIS Real-time Analysis (TARA; Oct 20, 2005) software package.⁷ AE is ideal for extracting and analyzing the spectra of large numbers of point and diffuse sources observed with ACIS over multiple epochs. AE calls procedures from both CIAO (v3.3) and HEASOFT (v6.0.4) and uses calibration files that are part of the CALDB v3.2.1 product provided by the *Chandra* X-ray Center.

The ≈ 2 Ms CDF-N (≈ 1 Ms CDF-S) observations are comprised of 20 (10) event files. The event files were corrected for charge transfer inefficiency, bad columns, bad pixels, and cosmic ray afterglows. The event files were also filtered for time intervals of acceptable aspect solution and background levels. A detailed description of the data reduction procedures are presented in Alexander et al. (2003). Background event files and exposure maps were created by excluding circular regions centered on the detected sources with radii that are a factor of 1.1 times larger than the 99% encircled energy radii of the point spread functions at ~ 1.49 keV. Source extraction regions were constructed to contain 90% of the PSF encircled energy derived from the CXC 1.4967 keV PSF libraries. There were two exceptions to this procedure. First, for sources with greater than 1000 counts in the Alexander et al. (2003) catalog we used extraction regions that contained 99% of the PSF encircled energy.

⁵ In AGNs values of α_r could be flatter than the adopted $\alpha_r = 0.8$ (e.g., Richards et al. 1998; Muxlow et al. 2005), with measured standard deviations ~ 1 (e.g., Wadadekar 2004). We investigated how a flatter α_r may affect our results and find that choosing a value of $\alpha_r = 0.6$, for example, to estimate R will not change our sample of RQ AGNs, whereas, a value of $\alpha_r = 0.4$ will result in the exclusion of only two sources from our sample (1% of the entire sample) in order to satisfy $R \lesssim 10$. We conclude that our sample selection and results of our statistical analysis are not significantly affected by values of the radio spectral index as low as $\alpha_r = 0$.

⁶ The radio surveys of Richards (2000) and Afonso et al. (2006) cover the entire CDF-N and CDF-S regions respectively. More details of the CDF-S radio observations are found in Norris et al. (2006).

⁷ TARA is available at <http://www.astro.psu.edu/xray/docs/TARA/>

Second, for sources with 90% encircled energy extraction regions that overlapped we reduced the extraction regions to avoid overlap. Local background extraction regions were chosen as annuli centered on the source positions with inner radii equal to that of the source extraction regions and with outer radii selected such that the background region contained at least 100 background counts and had an area at least four times that of the source region.

We note that in the current analysis we made no attempt to correct for possible spectral variability over the few year period of the observations of the CDFs. Spectra obtained are therefore time-averaged over the period of the observations.

4. SPECTRAL ANALYSIS

Two energy bands were used to fit the *Chandra* spectra: the 0.5–8 keV observed-frame and the 2–10 keV rest-frame. To obtain the maximum S/N we utilized the observed-frame energy range of 0.5–8 keV. The lower energy bound was chosen because the *Chandra* effective area is not well calibrated below 0.5 keV, and the upper energy bound was chosen because the S/N decreases greatly above this energy for most of the sources in the sample. One advantage of using the same observed-frame energy range for every object is that the same systematic instrumental uncertainties apply to every fit. Since most of the detected spectrum is used in the analysis, the S/N is higher than for cases where restricted energy ranges were used.

To test how the $\Gamma - L_X$ correlation might be affected by absorption and possible contamination from other emission processes, we also fitted the spectra in the rest-frame energy range of 2–10 keV. This range was selected to avoid possible contamination from soft-excess emission that is often detected in AGNs below rest-frame energies of ~ 1 keV. The selection of the 2–10 keV rest-frame band also aids in reducing the effects of X-ray absorption. For example, assuming a source with a power-law spectrum of $\Gamma = 1.7$, $z = 1$, $N_H \sim 10^{22} \text{ cm}^{-2}$, and solar abundances the fraction of absorbed photons is 30% in the 0.5–8 keV observed-frame band and 9% in the 2–10 keV rest-frame band. The 2–10 keV rest-frame also minimizes possible contamination from Compton-reflection emission from circumnuclear material that is thought to peak at a rest-frame energy of about 20 keV. In general, 2–10 keV rest-frame spectra have fewer counts than 0.5–8 keV observed-frame spectra. For fits performed in the 2–10 keV rest-frame band, we selected sources with more than 170 counts in this band, leaving a sub-sample of 144 RQ AGNs.

The total number of photon counts per source (S) with energies in the 0.5–8 keV observed-frame band lies in the range 170–13000. In Figure 1 (lower panel) we present the number of $z > 0.1$ radio-quiet AGNs in our sample versus the number of photons with energies in the 0.5–8 keV observed-frame band. The solid line applies to sources with spectral fits performed in the 0.5–8 keV observed-frame, and the dotted line applies to sources with spectral fits performed in the 2–10 keV rest-frame. The mean logarithm of S for sources with spectral fits performed in the 0.5–8 keV observed-frame is $\langle \log S \rangle = 2.74$ with a standard deviation of $\sigma \simeq 0.42$. The mean logarithm of S for sources with spectral fits

TABLE 1
MODELS USED IN FITTING THE SPECTRA OF THE RQ AGNs OF
OUR SAMPLE.^a

Model ^b	No sources	% of the whole sample
PL	77	44.5
APL	76	43.9
PAPL	9	5.2
IAPL	4	2.3
PL+EL	4	2.3
APL+EL	3	1.7

^a The selection criteria for the sample of RQ AGNs of our present study were that the redshifts of the sources were greater than 0.1 and the total number of photons in the full band (0.5–8 keV) was greater than ~ 170 .

^b PL \equiv power-law (XSPEC model wabs(pow)); APL \equiv absorbed power-law (XSPEC model wabs*zwabs(pow)); PAPL \equiv partially absorbed power-law (XSPEC model wabs*zpcfabs(pow)); IAPL \equiv ionized absorbed power-law (XSPEC model wabs*absori(pow)); PL+EL \equiv power-law + emission-line (XSPEC model wabs(pow+zgauss)); APL+EL \equiv absorbed power-law + emission-line (XSPEC model wabs*zwabs*(pow+zgauss)).

performed in the 2–10 keV rest-frame is $\langle \log S \rangle = 2.83$ with a standard deviation of $\sigma \simeq 0.41$. Based on the fact that our sample contains sources with relatively low counts, we used the C -statistic (Cash 1979) to fit spectra as adopted in a similar study presented in Tozzi et al. (2006). In this study, the authors concluded that the C -statistic is more accurate than the χ^2 -statistic in estimating the spectral parameters of AGNs with low-count spectra (~ 100 counts); similar arguments are presented in Nousek & Shue (1989). We also performed spectral fits in the 0.5–8 keV observed-frame band using the χ^2 -statistic, with a grouping of 10 counts per bin. The sole purpose of using the χ^2 -statistic was to apply the F -test to assess the use of more complex spectral models.

For the CDF-S and CDF-N sources of our sample, we assumed Galactic column densities of $8.8 \times 10^{19} \text{ cm}^{-2}$ (Stark et al. 1992) and $1.3 \times 10^{20} \text{ cm}^{-2}$ (Lockman 2004), respectively. The spectral analysis was performed using XSPEC version 12. The default spectral model used is a power law (PL; POW) with Galactic absorption (WABS). Additional model components were added to the default model in cases where the F -test showed an improvement in the fit at the 95% confidence level (0.5–8 keV observed-frame) when these additional components were used. We refer to models comprised of the default model plus additional model components as alternative models. Alternative models included an absorbed-power-law model (APL) at the redshift of the source (WABS ZWABS POW), an ionized-absorbed-power-law model (IAPL) (WABS ABSORI POW), a partial-absorbed-power-law model (PAPL) (WABS ZPCFABS POW) and/or models that included an iron line (PL+EL; APL+EL) (WABS ZGAUSS POW; WABS ZWABS ZGAUSS POW). We also considered models that contained a Compton-reflection component (PEXRAV), but we did not find any improvement in the fits using such models. Our finding, that none of the sources in our sample require a Compton-reflection component, is in agreement with Tozzi et al. (2006) who find that only 14 out of 321 CDF-S sources require Compton-reflection components. We note that none of these 14 sources are part of our sample mostly because they con-

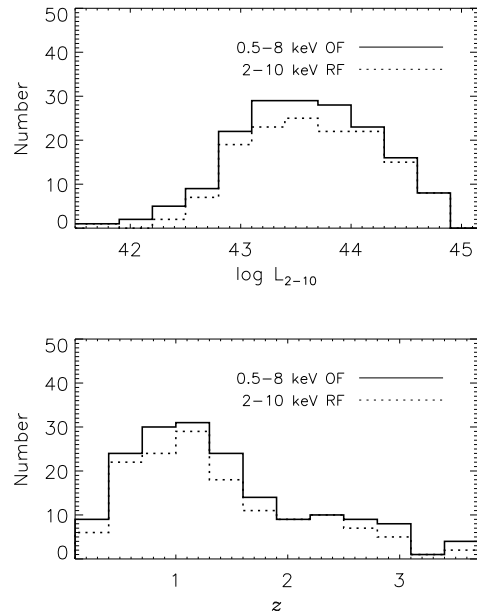


Fig. 2.— Number of sources vs. luminosity (upper panel) and redshift (lower panel). The solid line represents sources with fits performed in the 0.5–8 keV observed-frame band and the dotted line represents sources with fits performed in the 2–10 keV rest-frame band.

tain less than 170 counts. Even though we do not detect a significant reflection-component in our spectral fits, an unaccounted reflection-component could still be affecting the estimation of Γ (see §5.2.6 for details). In Table 1, we list the number of sources from our sample (the entire sample contains 173 RQ AGNs) fit with a particular spectral model. From Table 1, we notice that based on the F -test there are 92 sources with detected absorption (~ 53 % of the whole sample) and 7 cases with detected iron lines (~ 4 % of the whole sample).

The spectral-fitting results are presented in Table 2 for fits performed in the 0.5–8 keV observed-frame band (173 RQ AGNs), and the fits performed in the 2–10 keV rest-frame band (144 RQ AGNs). In Table 2 we provide the photon index Γ (errors at the 90% confidence level), the intrinsic column density N_{H} (errors at the 90% confidence level) in units of 10^{22} cm^{-2} , and the logarithm of the hard X-ray luminosity in the rest-frame 2–10 keV band in units of erg s^{-1} (hereafter referred to as L_{2-10}). Table 2 also includes the X-ray identification of the sources based on their RA and DEC positions, the photon counts in the fitted range, the number of degrees of freedom, and the values of the C -statistic. The last two quantities provide an estimate of the quality of the fits.

In Figure 2, we show the distributions of 2–10 keV luminosities (upper panel) and redshifts (lower panel) of the sources in our sample with fits performed in the 0.5–8 keV observed-frame band (solid line; 173 RQ AGNs) and the 2–10 keV rest-frame band (dotted line; 144 RQ AGNs). The luminosities of the sources in our sample cover the range $3 \times 10^{41} - 6 \times 10^{44} \text{ erg s}^{-1}$ where the lower limit is mostly determined by the sensitivity limit of the CDF-N survey, while the upper limit is a statistical consequence of the fact that luminous AGNs

TABLE 2
 PROPERTIES OF OUR SAMPLE OF RQ AGNS SELECTED FROM THE CHANDRA DEEP FIELD SURVEYS.

Xid ^a	z ^b	Counts ^c	Γ	N_{H}^{d}	$\log L_{2-10}$	C -stat	dof	type ^e	model ^f
RESULTS BASED ON FITS PERFORMED IN THE 0.5–8 KEV OBSERVED-FRAME.									
CXOJ123521.32+621628.1	0.559 ^{sp}	513.4	$1.51^{+0.17}_{-0.07}$..	42.79	519.2	510	non-type 1	PL
CXOJ123528.77+621427.8	0.850 ^{ph}	183.2	$1.19^{+0.92}_{-0.42}$	$4.95^{+4.59}_{-1.97}$	43.06	542.0	509	non-type 1	APL
CXOJ123529.45+621822.8	3.000 ^{ph}	205.8	$0.81^{+0.24}_{-0.24}$..	43.93	516.1	510	non-type 1	PL
CXOJ123535.21+621429.1	2.240 ^{ph}	310.5	$1.64^{+0.32}_{-0.42}$	$2.57^{+1.86}_{-2.57}$	43.80	467.8	509	non-type 1	APL
CXOJ123537.10+621723.6	2.050 ^{sp}	451.1	$1.82^{+0.21}_{-0.16}$..	43.95	488.5	510	type 1	PL
CXOJ123539.14+621600.3	2.575 ^{sp}	729.8	$1.91^{+0.25}_{-0.16}$	$1.98^{+0.88}_{-1.15}$	44.33	489.1	509	type 1	APL
CXOJ123546.07+621559.9	1.930 ^{ph}	242.6	$1.09^{+0.20}_{-0.20}$..	43.49	474.8	510	non-type 1	PL
CXOJ123548.37+621703.3	0.850 ^{ph}	396.8	$1.66^{+0.15}_{-0.15}$..	42.92	440.5	510	non-type 1	PL
CXOJ123548.53+621931.2	3.100 ^{ph}	226.0	$1.22^{+0.26}_{-0.15}$..	43.95	439.5	510	non-type 1	PL
CXOJ123550.42+621808.6	1.300 ^{ph}	955.9	$1.41^{+0.15}_{-0.16}$	$2.04^{+0.69}_{-0.62}$	43.95	518.3	509	non-type 1	APL
RESULTS BASED ON FITS PERFORMED IN THE 2–10 KEV REST-FRAME.									
CXOJ123521.32+621628.1	0.559 ^{sp}	320.5	$1.49^{+0.23}_{-0.23}$..	42.80	386.6	349	non-type 1	PL
CXOJ123535.21+621429.1	2.240 ^{ph}	256.7	$1.89^{+0.70}_{-0.62}$	$3.18^{+3.68}_{-3.18}$	43.81	176.0	165	non-type 1	APL
CXOJ123537.10+621723.6	2.050 ^{sp}	365.7	$1.88^{+0.24}_{-0.23}$..	43.94	220.0	177	type 1	PL
CXOJ123539.14+621600.3	2.575 ^{sp}	604.0	$1.84^{+0.42}_{-0.40}$	$1.96^{+2.20}_{-1.96}$	44.33	161.0	149	type 1	APL
CXOJ123546.07+621559.9	1.930 ^{ph}	182.6	$0.85^{+0.33}_{-0.33}$..	43.53	218.8	184	non-type 1	PL
CXOJ123548.37+621703.3	0.850 ^{ph}	261.3	$1.69^{+0.26}_{-0.24}$..	42.91	268.3	293	non-type 1	PL
CXOJ123550.42+621808.6	1.300 ^{ph}	789.5	$1.69^{+0.23}_{-0.36}$	$3.49^{+1.10}_{-1.62}$	43.99	274.8	234	non-type 1	APL
CXOJ123551.75+621757.1	1.910 ^{ph}	1016.8	$1.65^{+0.30}_{-0.28}$	$1.67^{+1.32}_{-1.21}$	44.37	179.0	181	non-type 1	APL+EL
CXOJ123553.13+621037.3	1.379 ^{sp}	1329.0	$1.85^{+0.19}_{-0.30}$	$0.88^{+0.91}_{-0.71}$	44.22	225.8	226	type 1	APL
CXOJ123555.08+621610.7	1.022 ^{sp}	188.7	$1.25^{+0.80}_{-0.38}$	$14.88^{+13.25}_{-9.43}$	43.29	341.0	266	non-type 1	PAPL

Note.— Table 2 is presented in its entirety in the electronic edition of the *Astronomical Journal*. A portion is shown here for guidance regarding its form and content.

^a Xid with RA+DEC coordinates.

^b Spectroscopic (sp) and photometric (ph) redshifts gathered from the literature (see §2).

^c Background subtracted source counts in the 0.5–8 keV observed-frame band for fits performed in the 0.5–8 keV observed-frame band and counts in the 2–10 keV rest-frame band for fits performed in the 2–10 keV rest-frameband.

^d In units of 10^{22} cm^{-2} .

^e Based on Bauer et al. (2004a), source classifications from §4.1.1 (<http://www.astro.psu.edu/~niel/hdf/hdf-chandra.html>)

^f PL≡power-law (XSPEC model wabs(pow)); APL≡absorbed-power-law (XSPEC model wabs*zwabs(pow)); PAPL≡partially-absorbed-power-law (XSPEC model wabs*zpcfabs(pow)); IAPL ≡ionized-absorbed-power-law (XSPEC model wabs*absori(pow)); PL+EL≡power-law + emission-line (XSPEC model wabs(pow+zgauss)); APL+EL≡absorbed-power-law + emission-line (XSPEC model wabs*zwabs*(pow+zgauss)).

^g The estimated values of Γ , N_{H} , and X-ray luminosities presented in this table are based on spectral fits performed in the 0.5–8 keV observed-frame.

($L_{2-10} \gtrsim 10^{45} \text{ erg s}^{-1}$) are less numerous than lower luminosity AGNs (see e.g., Brandt & Hasinger 2005). The mean redshift and mean logarithmic X-ray luminosity of the sources with fits performed in the 0.5–8 keV observed-frame band are $\langle z \rangle \simeq 1.41$ and $\langle \log L_{2-10} \rangle \simeq 43.6$, respectively. The mean redshift and mean logarithmic X-ray luminosity of the sources with fits performed in the 2–10 keV rest-frame band are $\langle z \rangle \simeq 1.38$ and $\langle \log L_{2-10} \rangle \simeq 43.6$, respectively.

In Figure 3 (upper panel), we show the distributions of the photon indices of the sources with fits performed in the 0.5–8 keV observed-frame band (solid line) and the 2–10 keV rest-frame band (dotted line). We find the mean photon indices and their standard deviations for fits performed in the 0.5–8 keV observed-frame and

2–10 keV rest-frame bands to be $\langle \Gamma \rangle \simeq 1.60 \pm 0.27$ and $\langle \Gamma \rangle \simeq 1.70 \pm 0.29$, respectively. In Figure 3 (lower panel), we show the distributions of the intrinsic column densities of sources with significant absorption (only sources where the F -test indicated significant intrinsic absorption at the >95% confidence level are included in the distributions); sources with fits performed in the 0.5–8 keV observed-frame band are indicated with the solid line (92/173), and sources with fits performed in the 2–10 keV rest-frame band are indicated with the dotted line (82/144). In the two fitted energy ranges, the peak of intrinsic column density distribution is $\log N_{\text{H}} \sim 22.6$, and there is a fraction of $\sim 40\%$ sources from the total sample having $\log N_{\text{H}} > 22$. We note that there are likely systematic errors on these column density es-

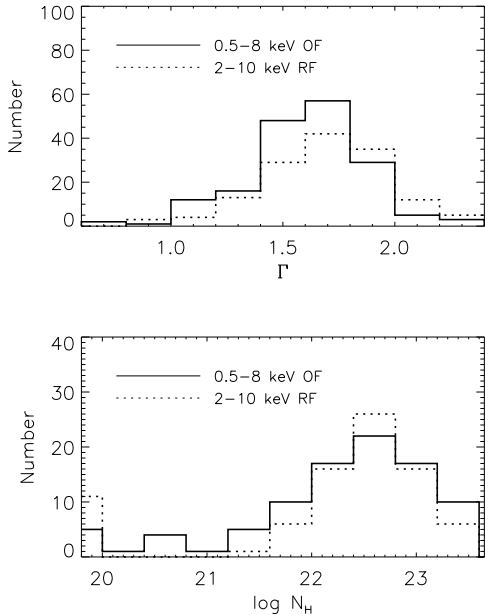


FIG. 3.— Number of sources vs. photon index (upper panel) and column density (lower panel). In the lower panel we show only the sources with a significant detection of absorption in their spectra. The solid line represents sources with fits performed in the 0.5–8 keV observed-frame band and the dotted line represents sources with fits performed in the 2–10 keV rest-frame band.

timates due to unmodeled absorption complexity. These parameter values and distributions are in agreement with those found in Tozzi et al. (2006) and Dwelly & Page (2006).

In Figure 4, we present a diagram comparing estimates of Γ obtained from fits performed in the 2–10 keV rest-frame (Γ_{rest}) and fits in the 0.5–8 keV observed-frame (Γ_{obs}). The size of each symbol in Figure 4 increases with redshift. Deviations from the straight line ($\Gamma_{\text{obs}} = \Gamma_{\text{rest}}$) are most likely statistical in nature, however, a few may be associated with the effects of intrinsic absorption, soft excesses, non-detected spectral lines, and Compton reflection.

In general, the agreement between Γ_{rest} and Γ_{obs} is good; this is first quantified by a high Pearson linear correlation coefficient (~ 0.73) and a very low null hypothesis probability ($\sim 4.8 \times 10^{-25}$). Secondly, this agreement is quantified by testing whether the linear relation between Γ_{rest} and Γ_{obs} is consistent with $\Gamma_{\text{rest}} = \Gamma_{\text{obs}}$. To verify the later we performed a χ^2 fit to the data assuming $\Gamma_{\text{rest}} = \alpha \Gamma_{\text{obs}}$, where α was a free parameter.⁸ We considered the errors in both variables Γ_{rest} and Γ_{obs} when performing the least-squares fit. We obtained $\alpha = 0.996 \pm 0.08$ (error at the 68% confidence level) with $\chi^2 = 99.3$ for 143 degrees of freedom (dof). As a basic check for the luminosity dependence of the linear relation between Γ_{rest} and Γ_{obs} we performed χ^2 fits of the model $\Gamma_{\text{rest}} = \alpha \Gamma_{\text{obs}}$ to sources with $\log L_{2-10} \lesssim 43.6$ and sources with $\log L_{2-10} \gtrsim 43.6$.

⁸ A χ^2 fit using the relation $y = \alpha x$ to model some bivariate sample (x_i, y_i) with errors in both variables $(\sigma_{x_i}, \sigma_{y_i})$ is obtained by minimizing $\chi^2 = \sum_i \frac{(y_i - \alpha x_i)^2}{\sigma_{y_i}^2 + \alpha^2 \sigma_{x_i}^2}$

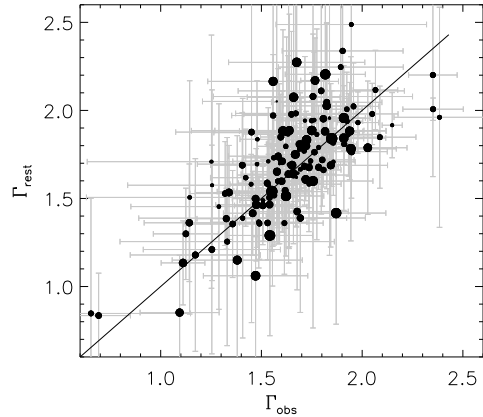


FIG. 4.— Spectral index for fits performed in the 2–10 keV rest-frame band (Γ_{rest}) versus spectral index for fits performed in the 0.5–8 keV observed-frame band (Γ_{obs}). The size of each symbol increases with redshift. The solid line represents the case of $\Gamma_{\text{obs}} = \Gamma_{\text{rest}}$. Notice that values of Γ_{rest} and Γ_{obs} can be found in Table 2.

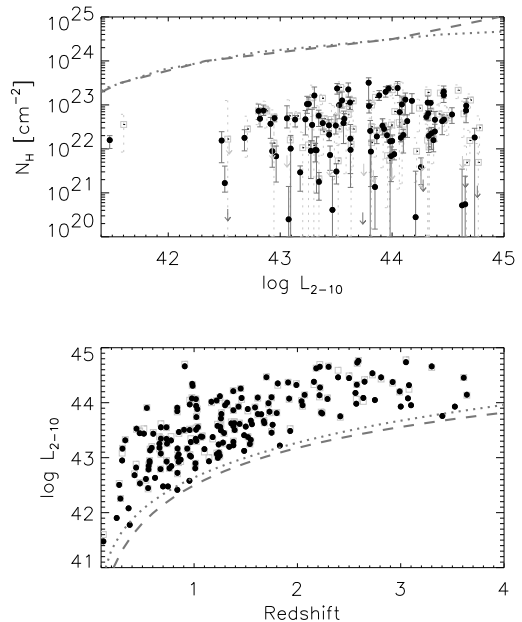


FIG. 5.— Estimated best-fit column densities versus 2–10 keV luminosities (upper panel), and 2–10 keV luminosities versus redshifts (lower panel) of the $z > 0.1$ RQ AGNs. Filled circles represent sources with fits performed in the 0.5–8 keV observed-frame band and open squares represent sources with fits performed in the 2–10 keV rest-frame band. In the upper panel, the two lines indicate the maximum column density that can be detected for a source with $0.1 \leq z \leq 4.0$, and a total of 170 counts in the 0.5–8 keV observed-frame (dashed) and 2–10 keV rest-frame (dotted). In the lower panel the lines indicate the minimum luminosity required for the detection of a source as a function of redshift. A total of 170 counts in the 0.5–8 keV observed-frame band (dashed) or a total of 170 counts in the 2–10 keV rest-frame band (dotted) is assumed. For the limits shown in this figure it is assumed that the source is detected at the ACIS-I aim-point with an exposure time of ≈ 2 Ms.

We obtained $\alpha = 0.995 \pm 0.011$ ($\chi^2 = 43.8$; dof=70) for sources with $\log L_{2-10} \lesssim 43.6$ and $\alpha = 0.997 \pm 0.010$ ($\chi^2 = 55.6$; dof=72) for sources with $\log L_{2-10} \gtrsim 43.6$.

5. RESULTS AND DISCUSSION

5.1. Selection Effects.

We begin this section by describing several selection effects that are intrinsic to our sample. Having an exposure of ≈ 2 times greater than the CDF-S survey, the CDF-N survey drives the sensitivity limits of our sources, so the following discussion will be focused on this survey.

Figure 5 shows the estimated best-fit column density versus the 2–10 keV luminosity (upper panel), and the 2–10 keV luminosity versus redshift (lower panel), for our $z > 0.1$ RQ AGNs. Spectral fits performed in the 0.5–8 keV observed-frame band and 2–10 keV rest-frame band are shown with filled circles and open squares respectively. In the upper panel of Figure 5, the dashed line shows the maximum column density that can be found for a source with $0.1 \leq z \leq 4.0$ assuming the source is detected at the ACIS-I aim-point with an exposure time of ≈ 2 Ms (Alexander et al. 2003) and a total of 170 counts in the 0.5–8 keV observed-frame band (dashed line) and 2–10 keV rest-frame band (dotted line). Each point on these curves is obtained by fixing N_H and finding the minimum luminosity that can be obtained with $0.1 \leq z \leq 4.0$ assuming a source with $\Gamma = 1.6$, Galactic column density of $1.3 \times 10^{20} \text{ cm}^{-2}$ and 170 counts in each fitted energy range. For low-luminosity sources ($L_{2-10} \lesssim 10^{42} \text{ erg s}^{-1}$), the threshold column density is $\approx 10^{24} \text{ cm}^{-2}$, which increases by a factor of ~ 10 for higher luminosity sources ($10^{44} - 10^{45} \text{ erg s}^{-1}$). The maximum column density observed at a specific luminosity is set by AGNs with $z = 0.1$ in most of the observed luminosity range; however, for luminous sources ($L_{2-10} \gtrsim 10^{44} \text{ erg s}^{-1}$) higher redshift AGNs ($z \sim 1-4$) establish the limit in N_H because these are less affected by absorption.

In the lower panel of Figure 5, the curves indicate the minimum luminosity required for the detection of a source as a function of redshift. We have assumed a source free of intrinsic absorption, positioned at the ACIS-I aim-point with an exposure time of ≈ 2 Ms, $\Gamma = 1.6$, galactic column density of $1.3 \times 10^{20} \text{ cm}^{-2}$ and with 170 photon counts in the 0.5–8 keV observed-frame (dashed line) or 170 counts in the 2–10 keV rest-frame (dotted line). The threshold luminosity is $\approx 10^{42} \text{ erg s}^{-1}$ for $z \approx 0.5$ and $\approx 3 \times 10^{43} \text{ erg s}^{-1}$ for $z \approx 2.5$. The dashed curve in Figure 5 is obtained by assuming no intrinsic absorption; however, the presence of N_H , which might be evolving (e.g., La Franca et al. 2005; Treister & Urry 2006; Tozzi et al. 2006), could be increasing the observed threshold luminosity.

5.2. Luminosity and Photon index

One of the goals of this work is to examine a possible correlation between L_X and Γ in a sample of RQ AGNs which was previously reported by Dai et al. (2004). To improve on the Dai et al. analysis we significantly increased the sample size using the CDFs, considered a larger redshift range, and used X-ray spectra that contained more than 170 counts in the full band (0.5–8 keV). The results of this analysis is shown in the following sections. For the following analysis we use the X-ray luminosity in the 2–10 keV rest-frame band (L_{2-10}).

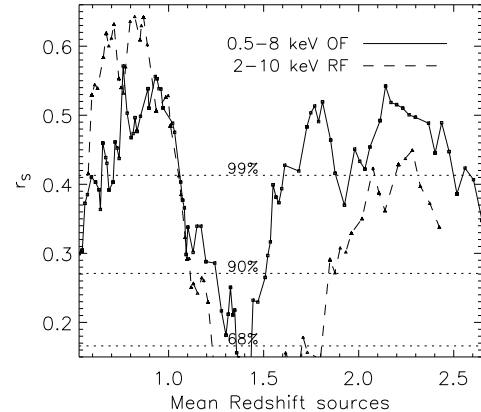


FIG. 6.— Spearman correlation coefficients of the $\Gamma - L_{2-10}$ relation as a function of the mean redshift within each sub-sample. Each sub-sample contains 38 RQ AGNs. The solid line corresponds to the fits performed in the 0.5–8 keV observed-frame band (Table 2). The dashed-line corresponds to the fits performed in the 2–10 keV rest-frame band (Table 2). The dotted lines correspond to three different levels of significance (68%, 90% and 99%), assuming 38 independent measurements of Γ vs. L_{2-10} .

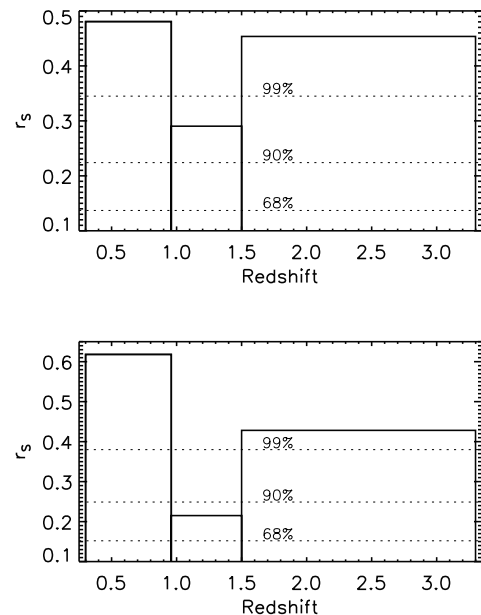


FIG. 7.— Spearman correlation coefficients of the $\Gamma - L_{2-10}$ relation as a function of redshift for the RQ AGNs within each independent redshift bin. In the upper panel each redshift bin contains ~ 55 RQ AGNs and the fits were performed in the 0.5–8 keV observed-frame band (Table 2). In the lower panel each redshift bin contains ~ 45 RQ AGNs, and the fits were performed in the 2–10 keV rest-frame band (Table 2). The dotted lines correspond to three different levels of significance (68%, 90% and 99%); these are obtained assuming 55 sources in the upper panel and 45 sources in the lower panel.

5.2.1. Possible evolution of the strength and significance of the $\Gamma - L_X$ correlation

As a first approach, we searched for a $\Gamma - L_X$ correlation as a function of redshift selecting sub-samples ordered in redshift. We used sub-samples containing 38 sources for fits performed in the 0.5–8 keV observed-

TABLE 3
CORRELATION TABLE OF Γ VERSUS L_X .

Cor. Coeff.	Redshift bin	Fitted Energy Range	Γ vs. L_{2-10}		
			N^a	r_C	% sign ^b
Spearman	$0.3 < z < 0.96$	0.5–8 keV observed-frame	53	0.48	>99.9
Kendall	$0.3 < z < 0.96$	0.5–8 keV observed-frame	53	0.33	>99.9
Pearson ^c	$0.3 < z < 0.96$	0.5–8 keV observed-frame	53	0.42	99.8
Spearman	$0.96 < z < 1.5$	0.5–8 keV observed-frame	54	0.29	96.7
Kendall	$0.96 < z < 1.5$	0.5–8 keV observed-frame	54	0.19	95.9
Pearson ^c	$0.96 < z < 1.5$	0.5–8 keV observed-frame	54	0.31	97.5
Spearman	$1.5 < z < 3.3$	0.5–8 keV observed-frame	57	0.45	>99.9
Kendall	$1.5 < z < 3.3$	0.5–8 keV observed-frame	57	0.32	>99.9
Pearson ^c	$1.5 < z < 3.3$	0.5–8 keV observed-frame	57	0.43	>99.9
Spearman	$0.3 < z < 0.96$	2–10 keV rest-frame	44	0.62	>99.9
Kendall	$0.3 < z < 0.96$	2–10 keV rest-frame	44	0.42	>99.9
Pearson ^c	$0.3 < z < 0.96$	2–10 keV rest-frame	44	0.530	>99.9
Spearman	$0.96 < z < 1.5$	2–10 keV rest-frame	46	0.22	84.9
Kendall	$0.96 < z < 1.5$	2–10 keV rest-frame	46	0.14	83.3
Pearson ^c	$0.96 < z < 1.5$	2–10 keV rest-frame	46	0.23	87.8
Spearman	$1.5 < z < 3.3$	2–10 keV rest-frame	48	0.43	99.8
Kendall	$1.5 < z < 3.3$	2–10 keV rest-frame	48	0.31	99.8
Pearson ^c	$1.5 < z < 3.3$	2–10 keV rest-frame	48	0.43	99.7

^a Number of RQ AGNs in each redshift bin.

^b Percentile significance of the correlation.

^c Calculated from Γ versus $\log L_X$.

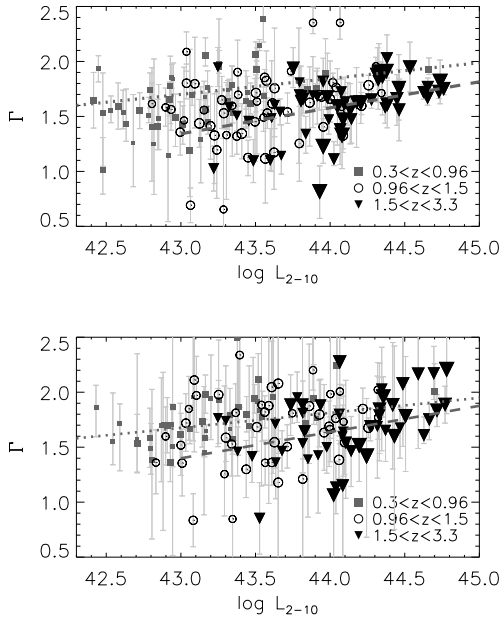


FIG. 8.— Γ versus 2–10 keV luminosity of radio-quiet AGNs in the redshift range of $0.3 < z < 3.3$. In the upper panel we show sources with fits performed in the 0.5–8 keV observed-frame band. In the lower panel we show sources with fits performed in the 2–10 keV rest-frame band. The symbol size increases with redshift. Filled squares are sources with $0.3 < z < 0.96$, open circles are sources with $0.96 < z < 1.5$, and filled triangles are sources with $1.5 < z < 3.3$. The dotted line indicates the least-squares fit to sources having $0.3 < z < 0.96$. The dashed line shows the least-squares fit to sources having $1.5 < z < 3.3$.

frame band and the 2–10 keV rest-frame band (Table 2). We calculated the mean redshift of each sub-sample and computed the Spearman rank correlation coefficient and significance of the correlation between Γ and L_{2-10} . This process was repeated by shifting the sampling window across the entire observed redshift range. Figure 6 shows

the values of the significance of the correlations and the Spearman correlation coefficients of the $\Gamma - L_{2-10}$ relation as a function of the mean redshift of the sources within each sub-sample, using the best-fit parameters from Table 2. The solid line in Figure 6 corresponds to sources fitted in the 0.5–8 keV observed-frame band and the dashed line corresponds to those fitted in the 2–10 keV rest-frame band. We notice that the correlation has two significant peaks ($\sim 99\%$) in both energy bands fitted, one with a mean redshift of ~ 0.7 , and the other with a mean redshift of ~ 2.2 .

As a second approach, we selected three independent redshift bins covering the redshift range $0.3 < z < 3.3$. The high redshift bin ($1.5 < z < 3.3$) was chosen to match the redshift range where Dai et al. (2004) found the $\Gamma - L_X$ correlation while the other two redshift bins ($0.3 < z < 0.96$ and $0.96 < z < 1.5$) were selected to obtain independent redshift bins with comparable numbers of sources within them. Each redshift bin contained ~ 55 sources in the 0.5–8 keV observed-frame band and ~ 45 sources in the 2–10 keV rest-frame band. In Figure 7 and Table 3 we show the Spearman rank correlation coefficient and the significance of the Spearman correlation coefficient in each bin. The upper panel of Figure 7 corresponds to fits performed in the 0.5–8 keV observed-frame and the lower panel to fits performed in the 2–10 keV rest-frame. The height of each bar is the significance of the $\Gamma - L_{2-10}$ Spearman correlation. The correlation for fits performed in the 0.5–8 keV observed-frame is significant for the three redshift bins; however, we find a slight decrease in the strength and significance in the second redshift bin for fits performed in the 2–10 keV rest-frame. The significance of the correlation in the first and third redshift bins is $>99.5\%$ for both fitting ranges. A significant expansion of our sample made by incorporating additional deep AGN surveys will be required to confirm the possible decrease of the strength of the correlation in the second redshift bin.

In Figure 8, we plot Γ vs. L_{2-10} for sources in each red-

shift bin of Figure 7, for fits performed in the 0.5–8 keV observed-frame (upper panel) and the 2–10 keV rest-frame (lower panel). Sources in our sample with redshifts in the range $0.3 \lesssim z \lesssim 0.96$ have a lower mean luminosity of $\langle \log L_{2-10} \rangle \sim 43.1$ ($\sigma_{\log L_{2-10}} \sim 0.5$) than sources with redshifts in the range $1.5 \lesssim z \lesssim 3.3$ which have a mean luminosity of $\langle \log L_{2-10} \rangle \sim 44.1$ ($\sigma_{\log L_{2-10}} \sim 0.4$). The luminosity distributions for sources in the redshift bins $0.3 \lesssim z \lesssim 0.96$ and $1.5 \lesssim z \lesssim 3.3$ are shown in Figure 9. We notice that the peak of the distribution of the sources in the high-redshift bin is significantly higher in luminosity than the peak of the distribution of the sources in the low-redshift bin. This shift in luminosity distributions is mainly a selection effect (see Figure 5) combined with the fact that luminous sources are more numerous at high redshift (Ueda et al. 2003; Hasinger et al. 2005). The Spearman correlation index of the $\Gamma - L_{2-10}$ data for the whole sample (173 RQ AGN) is ~ 0.24 (99.8% significance) and ~ 0.16 (94.1% of significance) for the 0.5–8 keV observed-frame and the 2–10 keV rest-frame spectral fits. These correlation coefficients are significantly lower than those found in the $0.3 \lesssim z \lesssim 0.96$ and $1.5 \lesssim z \lesssim 3.3$ redshift bins (see Table 3 for more details).

In Table 4, we show the results of a test of the $\Gamma - L_X$ correlation using only sources with spectroscopic redshifts. We find that the $\Gamma - L_X$ correlation of the sub-sample of sources with spectroscopic redshifts is significant in the three redshift bins; however, as indicated in Table 4, this sub-sample includes a larger fraction of type 1 AGNs and contains more sources with $\log N_H \lesssim 22$ than that of the whole sample. In addition, the size of this sub-sample is significantly smaller than the whole sample. We caution that the strengths of the correlations provided by the non-parametric tests used in our analysis of sub-samples containing a small number of sources N with the present uncertainties in the photon indices may be inaccurate since the variance of the Spearman correlation coefficient is $\sigma^2 = \frac{1}{N-1}$. Photometric redshifts are subject to larger errors than spectroscopic ones and for sources with $z > 1$ the error is approximately given by $\Delta z / (1+z) = 0.05$ (e.g. Cohen et al. 2000). In our analysis, the uncertainties in the redshifts will mainly affect the estimation of the X-ray luminosities. For example, a source at $z \sim 2$ will have an uncertainty in the estimated luminosity of $\Delta L_X / L_X \sim 0.3$. This level of uncertainty will not significantly affect our results since our study involves estimating changes in the photon index over two orders of magnitude in X-ray luminosity.

In the following three sections, we focus on sources in the first bin ($0.3 \lesssim z \lesssim 0.96$) and the third bin ($1.5 \lesssim z \lesssim 3.3$) and test the sensitivity of the $\Gamma - L_X$ correlation to the possible presence of intrinsic absorption and Compton reflection in the spectra of the sources.

5.2.2. Possible evolution of the slope and offset of the $\Gamma - L_X$ correlation

In Figure 10, we show Γ versus L_{2-10} for sources in the ranges of $0.3 \lesssim z \lesssim 0.96$ (upper panel), and $1.5 \lesssim z \lesssim 3.3$ (lower panel). The values of the X-ray luminosities and spectral indices shown in Figure 10 were obtained by fitting the spectra in the observed-frame energy range of 0.5–8 keV (see Table 2). We searched for a correlation between Γ and L_X by computing the Spearman’s and Kendall’s correlations (see Table 3). We find a strong cor-

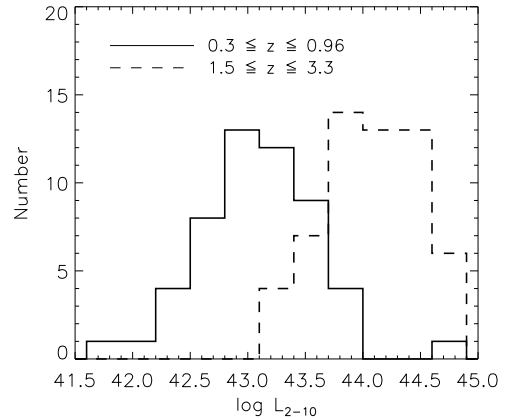


FIG. 9.— 2–10 keV rest-frame luminosity (L_{2-10}) distributions for radio-quiet AGNs with $0.3 \lesssim z \lesssim 1.5$ (thick line) and $1.5 \lesssim z \lesssim 3.3$ (dashed line). The fits are performed in the 0.5–8 keV observed-frame band.

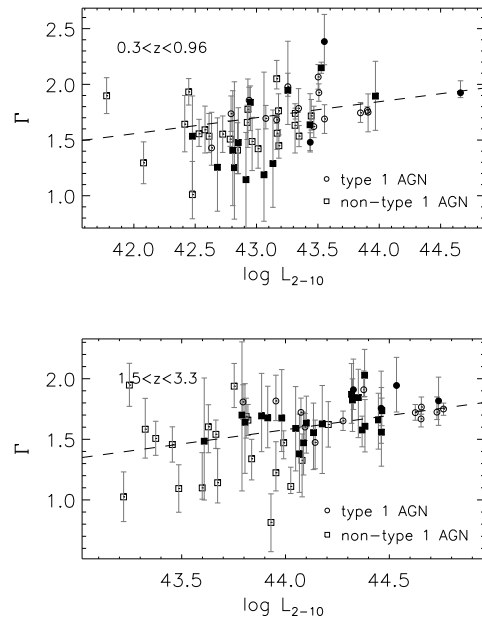


FIG. 10.— Γ versus 2–10 keV luminosity of radio-quiet AGNs with $0.3 \lesssim z \lesssim 0.96$ (upper panel) and with $1.5 \lesssim z \lesssim 3.3$ (lower panel). The values of the X-ray luminosities and spectral indices were obtained by fitting the spectra in the observed-frame energy range of 0.5–8 keV (see Table 2). The dashed lines indicate linear fits to the data using the least-squares method. The open symbols correspond to sources having $\log N_H \lesssim 22$, and the filled symbols are sources with $\log N_H > 22$. Circles correspond to type 1 AGNs and squares to non-type 1 AGNs.

relation between Γ and L_{2-10} , at the $>99.9\%$ confidence, for sources having $0.3 \lesssim z \lesssim 0.96$ and $1.5 \lesssim z \lesssim 3.3$. We tested for a linear dependence between Γ and $\log L_X$ by calculating the Pearson’s correlation and find a high significance ($>99.8\%$) for sources within $0.3 \lesssim z \lesssim 0.96$ and $1.5 \lesssim z \lesssim 3.3$ (see Table 3). In Table 5, we also present results of linear least-squares fits to the $\Gamma - L_X$ relation with a model of the form $\Gamma = \alpha \log L_X + \beta$. For this test, we assumed that Γ is the dependent variable with errors given at the 68% confidence level. In Table 5, we show the best-fit linear fit parameters α and β . We find

TABLE 4
CORRELATION TABLE OF Γ VERSUS L_X FOR AGNs WITH SPECTROSCOPIC REDSHIFTS.

Fitted Energy Frame	Redshift bin	N^a	Γ vs. L_{2-10}		fraction of type 1	fraction with $\log N_H \lesssim 22$
			r_C^b	% sign ^c		
0.5–8 keV observed-frame	$0.3 < z < 0.96$	46	0.47	99.9	0.37	0.70
2–10 keV rest-frame	$0.3 < z < 0.96$	40	0.64	>99.9	0.40	0.68
0.5–8 keV observed-frame	$0.96 < z < 1.5$	31	0.40	97.3	0.42	0.71
2–10 keV rest-frame	$0.96 < z < 1.5$	26	0.42	96.6	0.50	0.73
0.5–8 keV observed-frame	$1.5 < z < 3.3$	26	0.38	94.3	0.62	0.62
2–10 keV rest-frame	$1.5 < z < 3.3$	24	0.49	98.5	0.67	0.67

^a Number of RQ AGNs in each redshift bin.
^b Spearman correlation coefficient.
^c Percentile significance of the correlation.

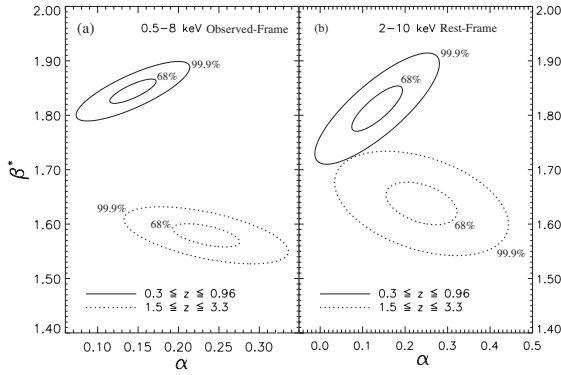


FIG. 11.— 68% and 99.9% confidence contours of the slope α and offset β^* of the $\Gamma - L_X$ correlation for AGNs in the $0.3 < z < 0.96$ (solid contours) and $1.5 < z < 3.3$ (dotted contours) redshift ranges. The parameters α and β^* were derived from fits of the linear model $\Gamma = \alpha \log \left(\frac{L_{2-10}}{10^{44} \text{ ergs/s}} \right) + \beta^*$. The fits were performed in the 0.5–8 keV observed-frame band (a) and in the 2–10 keV rest-frame band (b). The confidence contours indicate that the parameters of the linear fit to the $\Gamma - L_X$ correlation differ at the > 99.9% confidence level between the $0.3 < z < 0.96$ and $1.5 < z < 3.3$ redshift ranges.

that the best-fit parameters α and β show a significant change between the redshift bin $0.3 < z < 0.96$ and the redshift bins of $0.96 < z < 1.5$ and $1.5 < z < 3.3$. In particular, for spectral fits performed in the 0.5–8 keV observed-frame band we find the following: The slope and offset of the linear fit to the $\Gamma - L_X$ correlation in the $0.3 < z < 0.96$ redshift range are, $\alpha = 0.14 \pm 0.02$ and $\beta = -4.5 \pm 0.8$, respectively. The slope and offset of the $\Gamma - L_X$ correlation in the $1.5 < z < 3.3$ redshift range are, $\alpha = 0.23 \pm 0.03$, $\beta = -8.7 \pm 1.2$, respectively. Similar result are found for spectral fits performed in the 2–10 keV rest-frame. This change in the linear parameters can also be seen in Figure 8.

In Figure 11 we show the 68% and 99.9% confidence contours of α and β^* for AGNs in the $0.3 < z < 0.96$ and $1.5 < z < 3.3$ redshift ranges and for fits performed in the 2–10 keV rest-frame band (Figure 11a) and in the 0.5–8 keV observed-frame band (Figure 11b). The parameter β^* is obtained from fits of the model $\Gamma = \alpha \log \left(\frac{L_{2-10}}{10^{44} \text{ ergs/s}} \right) + \beta^*$. L_{2-10} was re-normalized for the purpose of illustrating better the full range of the contours. The 68% and 99.9% confidence contours levels correspond to $\Delta\chi^2(\alpha, \beta^*)$ values of 2.3 and 13.81, respectively. The confidence contours indicate that the parameters of the linear fit to the $\Gamma - L_X$ correlation change at the > 99.9% confidence level between the $0.3 < z < 0.96$

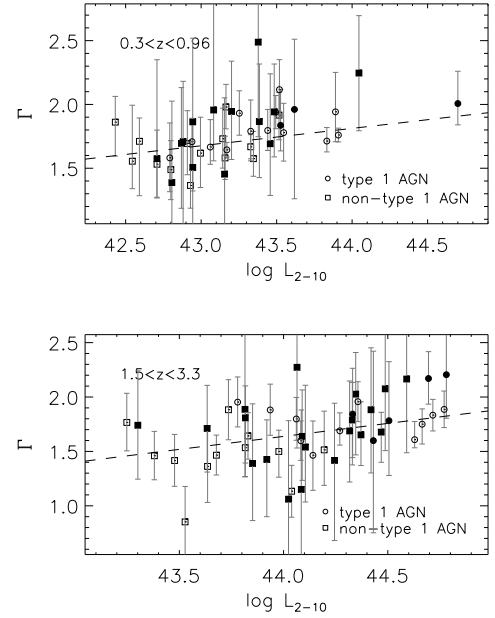


FIG. 12.— Γ versus 2–10 keV luminosity of radio-quiet AGNs with $0.3 < z < 0.96$ (upper panel) and with $1.5 < z < 3.3$ (lower panel). The values of the X-ray luminosities and spectral indices were obtained by fitting the spectra in the rest-frame energy range of 2–10 keV (see Table 2). The dashed lines indicate linear fits to the data using the least-squares method. The open symbols correspond to sources having $\log N_H \lesssim 22$, and the filled symbols are sources with $\log N_H > 22$. Circles correspond to type 1 AGNs and squares to non-type 1 AGNs.

and $1.5 < z < 3.3$ redshift ranges.

To test the sensitivity and stability of these confidence contours to possible outliers in the data we repeated the confidence contour analysis by excluding data points with significant deviations from the linear fit. In particular, we re-fit the $\Gamma - L_X$ correlation and re-calculated the confidence contours after excluding data points that deviated by more than 2σ , 2.5σ and 3σ from the linear fit. In all cases we find that the parameters of the linear fit to the $\Gamma - L_X$ correlation change between redshift bins 1 and 3 at the > 99.9% and > 98% confidence levels for fits performed in the 0.5–8 keV observed-frame and 2–10 keV rest-frame, respectively.

As discussed in §4 to test the influence of possible effects such as Compton reflection, soft excesses, and intrinsic absorption on the $\Gamma - L_X$ correlation, we also fitted the spectra in the 2–10 keV rest-frame, where these

TABLE 5
RESULTS OF LINEAR FITS TO THE Γ VS. LOG L_{2-10} RELATION. ^a

Redshift bin	Fitted energy range	Sample ^b	α	β
$0.3 \lesssim z \lesssim 0.96$	observed-frame 0.5–8 keV	CDFs	0.14 ± 0.02	-4.5 ± 0.8
$0.3 \lesssim z \lesssim 0.96$	rest-frame 2–10 keV	CDFs	0.13 ± 0.04	-4.1 ± 1.7
$0.96 \lesssim z \lesssim 1.5$	observed-frame 0.5–8 keV	CDFs	0.23 ± 0.03	-8.3 ± 1.5
$0.96 \lesssim z \lesssim 1.5$	rest-frame 2–10 keV	CDFs	0.27 ± 0.05	-9.9 ± 2.2
$1.5 \lesssim z \lesssim 3.3$	observed-frame 0.5–8 keV	CDFs	0.23 ± 0.03	-8.7 ± 1.2
$1.5 \lesssim z \lesssim 3.3$	rest-frame 2–10 keV	CDFs	0.24 ± 0.06	-8.9 ± 2.4
$1.5 \lesssim z \lesssim 3.3$	observed-frame 0.5–8 keV	combined	0.27 ± 0.03	-10.3 ± 1.2

^a Based on fits of a linear model ($\Gamma = \alpha \log L_{2-10} + \beta$) to the Γ versus $\log L_{2-10}$ relation, using the weighted least-squares method. The errors in Γ at the 68% level are used in the linear fit. L_{2-10} is the 2–10 keV rest-frame luminosity.

^b The CDFs sample consists of all the sources presented in Table 2. The combined sample consists of sources obtained from the independent surveys of Vignali et al. (1999), George et al. (2000), Reeves & Turner (2000), Page et al. (2003) and Dai et al. (2004) combined with the sources of our CDFs sample.

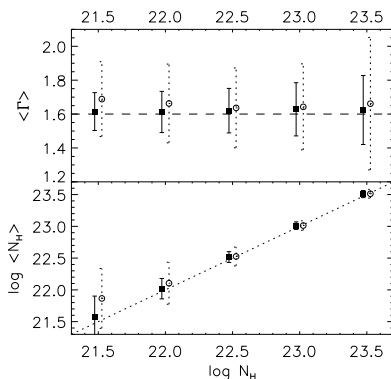


FIG. 13.— Results from fits performed on 1000 simulated spectra with $S = 550$, $\Gamma = 1.6$, $z=1.4$ and 5 different values of $\log N_H$ (21.5, 22, 22.5, 23 and 23.5). The estimated parameters with fits performed in the 0.5–8 keV observed-frame band are shown with filled squares (solid error bars), and the estimated parameters with fits performed in the 2–10 keV rest-frame band are shown with open circles (dashed error bars). A small shift in the value of $\log N_H$ (horizontal axis) has been introduced for visual purposes. In the upper panel we show $\langle \Gamma \rangle$ vs. $\log N_H$. In the lower panel we show $\log \langle N_H \rangle$ vs $\log N_H$. All error bars represent $\pm 1 \sigma$ deviations.

effects are expected to be smaller. The results of these spectral fits are presented in Table 2. In Figure 12, we present Γ versus L_{2-10} for sources in the redshift range of $0.3 \lesssim z \lesssim 0.96$ (upper panel), and in the redshift range of $1.5 \lesssim z \lesssim 3.3$ (lower panel) for spectral fits performed in the 2–10 keV rest-frame band. The results of our correlation analysis applied to the variables Γ and L_X are shown in Table 3. We find the Spearman, Kendall and Pearson correlation coefficients of Γ vs. L_{2-10} to be significant at the $>99.9\%$ and $>99.7\%$ confidence levels, for sources within $0.3 \lesssim z \lesssim 0.96$ and $1.5 \lesssim z \lesssim 3.3$ respectively. These results suggest that Compton reflection, soft excesses, and intrinsic absorption are most likely not driving the observed correlation between Γ and L_X in the two redshift bins analyzed in this section. In §5.2.3 and §5.3.6, we provide detailed analyses to show that intrinsic absorption and Compton reflection have negligible contributions to the $\Gamma - L_X$ correlation.

5.2.3. Dependence of the $\Gamma - L_X$ correlation on N_H

The estimated values of the photon indices used in our correlation analysis depend partially on the assumed

TABLE 6
RESULTS OF SIMULATIONS TO TEST THE PROBABILITY OF DETECTING INTRINSIC ABSORPTION THROUGH SPECTRAL FITS. ^a

$\log N_H$	Percentage of cases ^b
21.5	41.8 %
22.0	74.7 %
22.5	99.1 %
23.0	100.0 %
23.5	99.9 %

^a For each of the 5 different values of $\log N_H$ ($\log N_H = 21.5, 22, 22.5, 23$ and 23.5), we randomly generated 1000 fake spectra assuming sources close to the aim-point of the Chandra ACIS-I CCD, with 550 counts in the 0.5–8 keV band, $\Gamma = 1.6$, and $z = 1.4$.

^b Percentage of cases out of the 1000 simulated cases where the F -test indicates a significant presence of absorption assuming the input values of column densities listed in the first column.

spectral models used to fit the AGN spectra. In particular, the default model used in our spectral analysis assumes a simple power law that can be modified by intrinsic absorption. There is some evidence suggesting that the intrinsic column density (N_H) could be evolving both with X-ray luminosity (e.g, Ueda et al. 2003; Akylas et al. 2006) and redshift (e.g., Akylas et al. 2006; Treister & Urry 2006). At the same time, large values of N_H could be producing some dispersion in the estimated values of Γ . In order to analyze the effect of N_H in the spectral fitting, we have performed simulations using the software command “fakeit” in XSPEC. We randomly generated 1000 fake spectra for each of five values of N_H ($\log N_H = 21.5, 22, 22.5, 23$ and 23.5). Each simulated spectrum was created assuming an absorbed power-law (APL) model with 550 counts in the 0.5–8 keV band, $\Gamma = 1.6$, and $z = 1.4$. The simulated sources were considered close to the aim-point of the Chandra ACIS-I CCD. The assumed values of the total counts, Γ and z are close to the mean values found in §4. We performed fits to the randomly generated spectra using the same APL model, and plot in Figure 13 (upper panel), the mean spectral slope (with standard deviation) of the 1000 fits as a function of $\log N_H$; these fits were performed both in the 0.5–8 keV observed-frame (squares) and the 2–

TABLE 7
CORRELATION TABLE OF Γ VS. L_X FOR SUB-SAMPLES OF DIFFERENT ABSORPTION.

Redshift bin	Absorption ^a	Fitted energy range	N^b	L_{2-10} vs. Γ	
				r_C^c	% sign ^d
0.3	$\log N_H \lesssim 22.5$	0.5–8 keV observed-frame	40	0.38	98.4
0.3	$\log N_H \gtrsim 22.0$	0.5–8 keV observed-frame	37	0.38	98.1
0.3	$\log N_H \gtrsim 22.0$	0.5–8 keV observed-frame	16	0.66	99.4
0.3	type 1	0.5–8 keV observed-frame	17	0.34	81.6
0.3	$\log N_H \gtrsim 22.5$	2–10 keV rest-frame	32	0.56	>99.9
0.3	$\log N_H \gtrsim 22.0$	2–10 keV rest-frame	27	0.56	99.8
0.3	$\log N_H \gtrsim 22.0$	2–10 keV rest-frame	17	0.67	99.7
0.3	type 1	2–10 keV rest-frame	16	0.58	98.2
0.96	$\log N_H \gtrsim 22.5$	0.5–8 keV observed-frame	38	0.27	89.9
0.96	$\log N_H \gtrsim 22.0$	0.5–8 keV observed-frame	31	0.31	91.6
0.96	$\log N_H \gtrsim 22.0$	0.5–8 keV observed-frame	23	0.31	85.4
0.96	type 1	0.5–8 keV observed-frame	17	0.20	49.5
0.96	$\log N_H \gtrsim 22.5$	2–10 keV rest-frame	33	0.26	85.3
0.96	$\log N_H \gtrsim 22.0$	2–10 keV rest-frame	27	0.33	91.1
0.96	$\log N_H \gtrsim 22.0$	2–10 keV rest-frame	19	-0.18	54.8
0.96	type 1	2–10 keV rest-frame	16	0.15	37.1
1.5	$\log N_H \gtrsim 22.5$	0.5–8 keV observed-frame	40	0.45	99.7
1.5	$\log N_H \gtrsim 22.0$	0.5–8 keV observed-frame	32	0.35	95.2
1.5	$\log N_H \gtrsim 22.0$	0.5–8 keV observed-frame	25	0.38	94.2
1.5	type 1	0.5–8 keV observed-frame	16	0.12	34.0
1.5	$\log N_H \gtrsim 22.5$	2–10 keV rest-frame	34	0.45	99.2
1.5	$\log N_H \gtrsim 22.0$	2–10 keV rest-frame	23	0.42	95.6
1.5	$\log N_H \gtrsim 22.0$	2–10 keV rest-frame	23	0.42	96.2
1.5	type 1	2–10 keV rest-frame	16	0.29	72.1

^a Sub-samples contain RQ AGNs that are either type 1 AGN or have N_H less than a specified value.

^b Number of RQ AGNs in each sub-sample.

^c The Spearman correlation coefficient.

^d The significance of the Spearman correlation coefficient.

10 keV rest-frame (circles). Based on these results we do not find any significant bias in the estimation of Γ with N_H . We do, however, find that the standard deviation shows a clear tendency to grow with N_H independently of the energy band fit, as seen in Figure 13 (upper panel). In Figure 13 (lower panel), we see that in general the estimated value of N_H is accurate for $\log N_H \gtrsim 22$; however, for $\log N_H < 22$ the column density is slightly overestimated and has a larger dispersion.

Using the same simulations, we estimated the effectiveness of using the F -test at the 95% level of significance to determine the improvement in the fit quality by using an absorbed power-law (APL) model as an alternative to the default power-law (PL) model. Table 6 shows that in a simulation of 1000 fake spectra with $S = 550$, $\Gamma = 1.6$, $z = 1.4$ and $\log N_H = 22$, the F -test indicates absorption in $\sim 75\%$ of the spectra. For simulated spectra with $\log N_H = 22.5$, the F -test indicates absorption in $\sim 99\%$ of the cases and for $\log N_H > 22.5$ the F -test indicates absorption in more than 99.9% of the cases. Based on these simulations, we conclude that the F -test can accurately identify absorption when $\log N_H \gtrsim 22$.

Based on our finding that highly-absorbed sources show a greater dispersion of the estimated value of Γ , we tested the sensitivity of the $\Gamma - L_X$ correlation for sources having $0.3 \lesssim z \lesssim 0.95$ and $1.5 \lesssim z \lesssim 3.3$ to intrinsic absorption, by removing sources with significant absorption ($\log N_H \gtrsim 22.5$). We also tested this correlation for sources having $\log N_H < 22$. Finally as a complementary test we analyzed the $\Gamma - L_X$ correlation for type 1 AGNs. The results of these three tests are presented in Table 7. For sources having $\log N_H \lesssim 22.5$ and

$\log N_H \lesssim 22$ we find in the first and third redshift bins that the Spearman correlation coefficients of Γ versus L_{2-10} are significant at the $>95\%$ confidence levels. This result holds for sources with fits performed in both the 0.5–8 keV observed-frame and in the 2–10 keV rest-frame (see Table 7). Notice that sources having $\log N_H \lesssim 22$ are plotted as empty squares in Figures 10 and 12.

For type 1 AGNs, we find that the $\Gamma - L_{2-10}$ correlation is significant at the 82% and 12% levels in the first and third redshift bins, respectively, for fits performed in the 0.5–8 keV observed-frame band; the significances are at the 98% and 72% levels, respectively, for fits performed in the 2–10 keV rest-frame band. We briefly investigate possible reasons that may explain the apparent low detection significance of the $\Gamma - L_{2-10}$ relation for the type 1 AGNs of our sample. First we note that the luminosity ranges of the type 1 AGNs of our sample in the first and third redshift bins are $42.6 \lesssim \log L_{2-10} \lesssim 44.7$ and $43.8 \lesssim \log L_{2-10} \lesssim 44.8$. Our sample of type 1 AGNs therefore includes relatively luminous sources in each redshift bin. For sources in the third redshift bin, as we will later see in §5.2.7, the values of Γ appear to saturate above $\log L_{2-10} \sim 45$. Therefore, the type 1 AGNs detected in the third redshift bin of our sample are expected to lie on the flat part of the $\Gamma - L_X$ relation. We conclude that the apparent low significance of the $\Gamma - L_{2-10}$ relation for the type 1 AGNs of our sample found in the third redshift bin is mainly the result of their relatively large luminosity and the limited number of type 1 AGNs in our sample. Based on the tests presented in this section we confirm that the strong $\Gamma - L_X$ correlations that we find in RQ AGNs in the red-

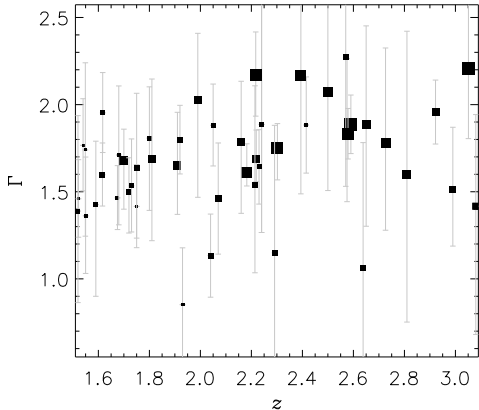


FIG. 14.— Spectral slope (Γ) versus redshift (z) of radio-quiet AGNs with $1.5 \lesssim z \lesssim 3.3$ with fits performed in the 2–10 keV rest-frame. The size of the symbols increases with L_{2-10} .

shift ranges of $0.3 \lesssim z \lesssim 0.95$ and $1.5 \lesssim z \lesssim 3.3$ are not driven by intrinsic absorption.

5.2.4. Other Correlations

We searched in the redshift ranges of $0.3 \lesssim z \lesssim 0.95$ and $1.5 \lesssim z \lesssim 3.3$ for possible correlations between the photon index Γ and other physical parameters of our sample of AGNs by computing Spearman rank correlations. The results from this correlation analysis are shown in Table 8. In the cases where the intrinsic column densities were $N_{\text{H}} \lesssim 10^{20} \text{ cm}^{-2}$, we could only obtain upper limits to N_{H} , and therefore computed the correlation coefficients using survival analysis (Isobe et al. 1986).

The selection criteria used in this work impose a luminosity limit which is redshift dependent (see Figure 5). Furthermore, the co-moving density of luminous AGNs is known to increase with z . These two effects will produce a correlation between L_{X} and z as can be seen in Table 8. We do not find any significant correlation between Γ and N_{H} in any bin. The fact that Γ is not correlated with N_{H} provides further support that the $\Gamma - L_{\text{X}}$ correlation is not driven by N_{H} .

We also find a weak correlation between N_{H} and z in the redshift range of $1.5 \lesssim z \lesssim 3.3$ for fits in the 2–10 keV rest-frame band. This result may imply that the intrinsic column density evolves, increasing with redshift. Such a result has been reported in several studies (e.g., La Franca et al. 2005; Treister & Urry 2006); however, the evolution of N_{H} with z is still a debatable topic since other authors have not found definitive evidence for the evolution in the “obscuration fraction” (e.g., Ueda et al. 2003; Akylas et al. 2006; Dwelly & Page 2006).

A rather surprising result was the detection of a correlation between Γ and z in the third redshift bin with an apparent significance of 99.6%. A careful analysis indicates that this apparent $\Gamma - z$ correlation is most likely the result of selection effects. This tendency seems to be confirmed in Figure 14. This Γ versus z plot indicates that higher luminosity sources tend to group in the upper right area and lower luminosity sources in the lower left area. To test for selection effects, we performed a correlation analysis including sources with luminosities greater than the minimum luminosity of a detectable source at $z \sim 3$. This limit corresponds to $\log L_{2-10} \sim 44$ (see Fig-

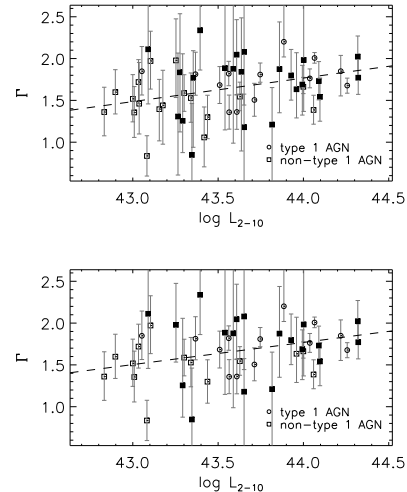


FIG. 15.— Γ versus 2–10 keV luminosity of radio-quiet AGNs having $0.96 \lesssim z \lesssim 1.5$ with fits performed in the 0.5–8 keV observed-frame band (upper panel) and fits performed in the 2–10 keV rest-frame band (lower panel). The dashed lines indicate linear fits to the data using the least-squares method. The open symbols represent sources having $\log N_{\text{H}} \lesssim 22$, and the filled symbols represent sources with $\log N_{\text{H}} > 22$. Circles represent type 1 AGNs and squares non-type 1 AGNs.

ure 5). We find that the Spearman’s correlation probability of the $\Gamma - z$ correlation in the third redshift bin for fits performed in the 2–10 keV rest-frame, decreases to a non-significant level of $\sim 66\%$ when we only include sources with $\log L_{2-10} \gtrsim 44$ (30 RQ AGNs). We note, however, that within the same luminosity range the $\Gamma - L_{2-10}$ correlation is significant at the $>99\%$ ($r_C \sim 0.6$) level. Our analysis indicates that the apparent correlation between Γ and z in the third redshift bin is most likely the result of selection effects. This conclusion is also confirmed in §5.2.7.

5.2.5. Radio-Quiet AGNs with $0.96 \lesssim z \lesssim 1.5$

In §5.2.1, we showed that the $\Gamma - L_{\text{X}}$ correlation was not significant for sources having $0.96 \lesssim z \lesssim 1.5$, especially for fits performed in the 2–10 keV rest-frame where we found that the correlation was only significant at the $\sim 85\%$ confidence level. In this section we investigate the cause of the lower significance of the $\Gamma - L_{\text{X}}$ relation for sources having $0.96 \lesssim z \lesssim 1.5$. In Figure 15, we show Γ versus L_{2-10} for sources having $0.96 \lesssim z \lesssim 1.5$ with fits performed in the 0.5–8 keV observed-frame (upper panel) and 2–10 keV rest-frame (lower panel). The Γ versus L_{2-10} data points show a larger scatter than what is seen in the other redshift bins consistent with the lower significance found for the $\Gamma - L_{\text{X}}$ correlation. In Table 7, we present the results of our correlation analysis of the $\Gamma - L_{\text{X}}$ data for sub-samples of different intrinsic absorption. We find that sources with $\log N_{\text{H}} \gtrsim 22$ and $0.96 \lesssim z \lesssim 1.5$ show no significant correlation between Γ and L_{X} , whereas sources with $\log N_{\text{H}} \lesssim 22$ and $0.96 \lesssim z \lesssim 1.5$ have a $\Gamma - L_{\text{X}}$ correlation that is significant at the $>90\%$ confidence level. We conclude that the absorbed sources with $0.96 \lesssim z \lesssim 1.5$ are possibly diluting the correlation significance found in this redshift bin. We caution, however, that the low number of sources per sub-sample used in this analysis combined with the uncertainties in the photon indices may result in inaccurate

TABLE 8
CORRELATION TABLE OF L_{2-10} VS. z , Γ VS. z , N_{H} VS. z , N_{H} VS. L_{2-10} AND Γ VS. N_{H} .

correlated parameters	N^a	Redshift bin	Fitted energy Range	r_c^b	% sign ^c	
L_{2-10} vs z	53	0.3	0.96	0.5–8 keV observed-frame	0.26	93.5
Γ vs z	53	0.3	0.96	0.5–8 keV observed-frame	0.12	61.4
N_{H} vs z	27	0.3	0.96	0.5–8 keV observed-frame	-0.08	30.9
N_{H} vs L_{2-10}	27	0.3	0.96	0.5–8 keV observed-frame	0.13	50.7
Γ vs N_{H}	27	0.3	0.96	0.5–8 keV observed-frame	0.14	53.6
L_{2-10} vs z	44	0.3	0.96	2–10 keV rest-frame	0.29	94.4
Γ vs z	44	0.3	0.96	2–10 keV rest-frame	0.23	87.4
N_{H} vs z	25	0.3	0.96	2–10 keV rest-frame	-0.05	20.6
N_{H} vs L_{2-10}	25	0.3	0.96	2–10 keV rest-frame	0.08	30.2
Γ vs N_{H}	25	0.3	0.96	2–10 keV rest-frame	0.32	88.5
L_{2-10} vs z	54	0.96	1.5	0.5–8 keV observed-frame	0.16	75.6
Γ vs z	54	0.96	1.5	0.5–8 keV observed-frame	-0.24	91.8
N_{H} vs z	28	0.96	1.5	0.5–8 keV observed-frame	-0.33	91.8
N_{H} vs L_{2-10}	28	0.96	1.5	0.5–8 keV observed-frame	-0.15	55.4
Γ vs N_{H}	28	0.96	1.5	0.5–8 keV observed-frame	-0.35	92.7
L_{2-10} vs z	46	0.96	1.5	2–10 keV rest-frame	0.17	74.6
Γ vs z	46	0.96	1.5	2–10 keV rest-frame	-0.08	41.1
N_{H} vs z	24	0.96	1.5	2–10 keV rest-frame	-0.36	91.3
N_{H} vs L_{2-10}	24	0.96	1.5	2–10 keV rest-frame	-0.10	36.0
Γ vs N_{H}	24	0.96	1.5	2–10 keV rest-frame	-0.03	11.8
L_{2-10} vs z	57	1.5	3.3	0.5–8 keV observed-frame	0.58	>99.9
Γ vs z	57	1.5	3.3	0.5–8 keV observed-frame	0.14	68.4
N_{H} vs z	34	1.5	3.3	0.5–8 keV observed-frame	0.13	53.5
N_{H} vs L_{2-10}	34	1.5	3.3	0.5–8 keV observed-frame	-0.23	81.8
Γ vs N_{H}	34	1.5	3.3	0.5–8 keV observed-frame	-0.11	48.3
L_{2-10} vs z	48	1.5	3.3	2–10 keV rest-frame	0.65	>99.9
Γ vs z	48	1.5	3.3	2–10 keV rest-frame	0.35	98.6
N_{H} vs z	30	1.5	3.3	2–10 keV rest-frame	0.34	93.4
N_{H} vs L_{2-10}	30	1.5	3.3	2–10 keV rest-frame	-0.02	8.8
Γ vs N_{H}	30	1.5	3.3	2–10 keV rest-frame	-0.1	40.4

^a Number of RQ AGNs in each sub-sample.

^b The Spearman correlation coefficient.

^c The significance of the Spearman correlation coefficient.

estimates of the strengths of the correlations.

Our correlation analysis between several other spectral parameters for sources with $0.96 \lesssim z \lesssim 1.5$ is included in Table 8. We find an anticorrelation between N_{H} and z at the $\sim 90\%$ confidence level for sources with $0.96 \lesssim z \lesssim 1.5$ and for fits performed in the 0.5–8 keV observed-frame and the 2–10 keV rest-frame bands. Correlations between Γ versus z and Γ versus N_{H} for sources in $0.96 \lesssim z \lesssim 1.5$ are found to be moderately significant for fits performed in the 0.5–8 keV observed-frame band and not significant for fits performed in the 2–10 keV rest-frame band.

5.2.6. Dependence of the $\Gamma - L_{\text{X}}$ correlation on Compton-reflection

In this section, we address the possibility that the $\Gamma - L_{\text{X}}$ correlation found in this work is produced by a change with luminosity of the Compton-reflection component. We note that the Compton-reflection component is difficult to model accurately in low-to-medium S/N X-ray spectra and therefore inaccurate modeling of this component may result in apparent flattening of the X-ray spectra.

Several studies indicate that the equivalent width (EW) of the iron $\text{K}\alpha$ emission line in the X-ray spectra of AGNs is anti-correlated with the 2–10 keV luminosity (e.g., Iwasawa & Taniguchi 1993; Nandra et al. 1997; Page et al. 2004a; Bianchi et al. 2007). This anti-correlation is commonly referred to as the ‘X-ray Baldwin effect’ and is also known as the ‘Iwasawa & Taniguchi

effect’. There are several proposed physical explanations in the literature for the X-ray Baldwin effect including (1) a change in the covering factor of a Compton-thick torus with luminosity (e.g., Konigl & Kartje 1994), (2) a luminosity-dependent ionization state of the iron-emitting material (e.g., Nandra et al. 1997), and (3) variability of the continuum AGN emission assuming constant iron-line fluxes (e.g., Jiang et al. 2006). It has also been proposed that the X-ray Baldwin effect is driven mostly by changes in the Eddington luminosity ratio rather than by X-ray luminosity (e.g., Jiang et al. 2006).

Several models of AGN accretion disks assume the iron line and Compton-reflection components originate from X-ray emission reprocessed in the accretion disk and indicate that the strength of the Compton-reflection component increases monotonically with the EW of the iron line (e.g., George & Fabian 1991; Ghisellini et al. 1994), and consequently decreases with L_{X} as well. Therefore, under this premise, these models could possibly explain the $\Gamma - L_{\text{X}}$ relation found in this work, since a decrease of the Compton-reflection component with L_{X} could result in an increase in Γ with L_{X} if the Compton-reflection component is not modeled accurately in our spectral analysis.

Bianchi et al. (2007) recently found a strong anti-correlation between the neutral narrow component of the iron $\text{K}\alpha$ emission line and the 2–10 keV luminosity of AGNs. These authors suggest that the neutral narrow iron-line component originates from the molecular torus and the broad iron-line component originates from reprocessing in the accretion disk. The dependencies,

however, of the Compton-reflection component with the 2–10 keV luminosity are still unclear (e.g., Nandra et al. 1995; Page et al. 2004b). It is also unclear whether the Compton-reflection component observed in the X-ray spectra of AGNs originates mostly from the torus or the accretion disk. If the neutral narrow iron $K\alpha$ emission line originates from the torus and the Compton-reflection component from the accretion disk then one cannot simply assume that the Compton-reflection component will follow the X-ray Baldwin effect. Variability studies of individual AGNs such as the Seyfert 1 galaxies NGC 5548 (Chiang et al. 2000) and MCG-6-30-15 (Lee et al. 2000) indicate that the Compton-reflection component increases with X-ray luminosity and the iron line EW and the relative normalization of the Compton-reflection hump are anti-correlated. We note that the Seyfert 1 galaxies in these variability studies were observed to vary over a factor of up to ≈ 3 in luminosity whereas our study includes objects spanning a factor of ~ 200 in luminosity. It is therefore difficult to extrapolate the results of these variability studies to our work.

Since observationally it is still unclear how the Compton-reflection component depends on X-ray luminosity we have investigated the degree to which Compton-reflection can be driving the $\Gamma - L_X$ relation by performing simulations and additional tests upon our data. We first simulated X-ray spectra containing Compton-reflection components with integer reflection scaling factors ranging between $0 \leq R \leq 4$. For each value of the reflection scaling factor ($R=0,1,2,3,4$); we simulated 1000 spectra using the FAKEIT command in XSPEC. The Compton-reflection components were simulated using the PEXRAV model, assuming sources close to the aimpoint of the ACIS-I CCD, $\Gamma=1.9$, $\log N_H = 22$, a total number of events per spectrum of $S=550$, an e-folding cutoff energy of $E_{cut}=400$ keV, and an inclination angle (i) of the reflector equal to 30° . The values of E_{cut} and i were chosen to be close to those generally used to model Seyfert galaxies (e.g., Magdziarz & Zdziarski 1995). Our results are insensitive to any reasonable value of E_{cut} and changing i will mostly affect the overall strength of the reflection component. We performed these simulations assuming redshifts of $z = 0.7$ and $z = 2.2$, which correspond to the mean redshifts of the sources in our sample with $0.3 \lesssim z \lesssim 0.96$ and $1.5 \lesssim z \lesssim 3.3$. We proceeded in fitting the simulated spectra with absorbed power-law models to estimate the decrease in the fitted values of Γ vs. the strength of the Compton-reflection component. In Figure 16 we show the best-fit values of Γ as a function of the reflection scaling factor for sources with redshifts of $z = 0.7$ (upper panel) and $z = 2.2$ (lower panel). In Figure 16 we also show the ratio of photons in the full band (0.5–8 keV) that originate from Compton reflection to photons from the direct power-law component (f_R).

As expected fits performed in the 2–10 keV rest-frame band of the high- z sources are less affected by the Compton-reflection component and show a smaller change of Γ than fits performed in the 0.5–8 keV observed-frame band. Specifically, we find apparent changes of Γ of about 0.7 and 0.3 for fits performed in the 0.5–8 keV observed-frame and 2–10 keV rest-frame bands, respectively, for sources with $1.5 \lesssim z \lesssim 3.3$.

Our simulations indicate that if Compton reflection

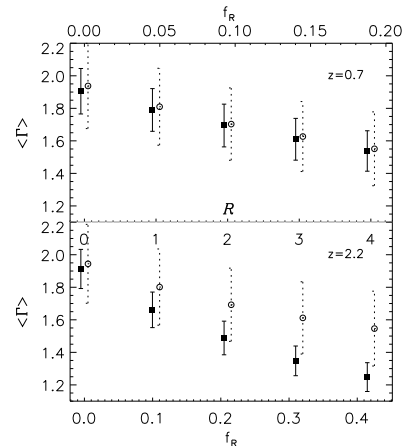


FIG. 16.— Results from fits performed on 1000 simulated spectra with $S=550$, $\Gamma=1.9$, and 5 different values of the Compton-reflection scaling factor R ($R=0,1,2,3,4$). The mean of the best-fit values of Γ with fits performed in the 0.5–8 keV observed-frame band are shown with filled squares (solid error bars), and the mean of the best-fit values of Γ with fits performed in the 2–10 keV rest-frame band are shown with open circles (dashed error bars). A small shift in the values of R (horizontal axis) has been introduced for visual purposes. In the upper panel we show $\langle \Gamma \rangle$ vs. R with $z=0.7$. In the lower panel we show $\langle \Gamma \rangle$ vs. R with $z=2.2$. On the x-axis we also show the ratio of photons (f_R) in the full band (0.5–8 keV) that originate from Compton reflection to photons that originate from the direct power-law component. All error bars represent $\pm 1 \sigma$ deviations.

is producing the observed change in Γ of about 0.5 for sources with $1.5 \lesssim z \lesssim 3.3$ (see lower panel of Figure 10), then the mean values of Γ derived from fits performed in the 0.5–8 keV observed-frame band should differ by about 0.2 from the mean values of Γ derived from fits performed in the 2–10 keV rest-frame band. Our observations indicate that this is not the case. For sources in the redshift bins of $0.3 \lesssim z \lesssim 0.96$, $0.96 \lesssim z \lesssim 1.5$ and $1.5 \lesssim z \lesssim 3.3$ the differences between the weighted mean values of Γ ($\langle \Gamma_{rest} \rangle - \langle \Gamma_{obs} \rangle$) obtained from fits performed in the 0.5–8 keV observed-frame and 2–10 keV rest-frame band are -0.03 ± 0.02 , 0.02 ± 0.02 and 0.01 ± 0.03 ($1-\sigma$ errors), respectively; the similarity between $\langle \Gamma_{rest} \rangle$ and $\langle \Gamma_{obs} \rangle$ is consistent with the results found in §4. According to our simulations, if the $\Gamma - L_X$ correlation were produced by the Compton-reflection component then these differences in the weighted mean values of Γ would increase with redshift, reaching values close to 0.2 for sources with $1.5 \lesssim z \lesssim 3.3$.

We also expect that if Compton reflection is driving the observed $\Gamma - L_X$ relation then the strength and slope of the correlation for fits performed in the 0.5–8 keV observed-frame band should be significantly stronger and steeper than the strength and slope of the correlation for fits performed in the 2–10 keV rest-frame band, especially for the high-redshift sources. This is not the case. As shown in Table 3, the strength of the $\Gamma - L_X$ relation in the 0.5–8 keV observed-frame and 2–10 keV rest-frame bands for sources with $1.5 < z < 3.3$ is 0.45 (at the 99.9% confidence level) and 0.43 (at the 99.8% confidence level), respectively. From Table 5 the ratio of the slopes of the $\Gamma - L_X$ relation for sources with $1.5 < z < 3.3$ is $\alpha_{obs}/\alpha_{rest} = 0.98 \pm 0.25$, where α_{obs} and α_{rest} are the slopes derived from fits performed in the 0.5–8 keV observed-frame and 2–10 keV rest-frame

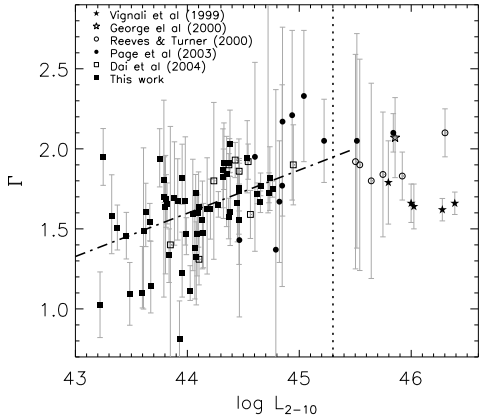


FIG. 17.— Photon indices of $1.5 \lesssim z \lesssim 3.3$ radio-quiet AGNs obtained from several surveys versus their 2–10 keV luminosities. Open stars are from Vignali et al. (1999), filled stars are from George et al. (2000), filled circles are from Reeves & Turner (2000), open circles are from Page et al. (2003), open squares are from Dai et al. (2004) and filled squares show data from this work. The vertical dashed line corresponds to $L_{2-10} = 2 \times 10^{45}$ erg s $^{-1}$. The dot-dashed line shows the best-fit linear model over the luminosity range of $10^{43} - 2 \times 10^{45}$ erg s $^{-1}$.

bands, respectively. Based on our simulations the ratio of the slopes of the $\Gamma - L_X$ relation for source with $1.5 < z < 3.3$ would be approximately $\alpha_{\text{obs}}/\alpha_{\text{rest}} \sim 1.5$ if Compton-reflection was driving the correlation.

5.2.7. Radio-Quiet AGNs from other surveys with $1.5 \lesssim z \lesssim 3.3$

We also tested the significance of the $\Gamma - L_X$ correlation in the redshift range of $1.5 \lesssim z \lesssim 3.3$ by combining results from the independent surveys of Vignali et al. (1999), George et al. (2000), Reeves & Turner (2000), Page et al. (2003), and Dai et al. (2004) with the results obtained from the CDFs. In Figure 17, we show Γ versus L_{2-10} for sources having $1.5 \lesssim z \lesssim 3.3$ combining the results of these surveys with our fits in the 0.5–8 keV observed-frame (Table 2). Sources from our survey fill in the low-luminosity range of the combined data $L_{2-10} \sim 10^{43} - 10^{45}$ erg s $^{-1}$. In this range Γ increases with L_X ; however, for $L_{2-10} \gtrsim 10^{45}$ erg s $^{-1}$ it appears that this relation begins to saturate.

We find that the Pearson linear correlation coefficient reaches a maximum value for sources with L_{2-10} in the range of $10^{43} - 2 \times 10^{45}$ erg s $^{-1}$, and the Spearman rank coefficient reaches a maximum value for sources with L_{2-10} in the range of $10^{43} - 8 \times 10^{45}$ erg s $^{-1}$. There are 76 sources with L_{2-10} in the range of $10^{43} - 2 \times 10^{45}$ erg s $^{-1}$. The Pearson’s correlation coefficient for $\Gamma - L_X$ in this luminosity range is $r_p \sim 0.52$ and is significant at the $>99.9\%$ confidence level (null hypothesis probability 1.8×10^{-6}). For reference, the values of the parameters of the best-fit model of the form $\Gamma = \alpha \log L_{2-10} + \beta$ can be found in Table 5. There are 84 sources with L_{2-10} in the range of $10^{43} - 8 \times 10^{45}$ erg s $^{-1}$. The Spearman correlation coefficient in this luminosity range is $r_s \sim 0.60$ and is significant at the $>99.9\%$ confidence level (null hypothesis probability $\sim 1.6 \times 10^{-9}$). The limits of the optimized ranges are marked in Figure 17. Figure 17 suggests two different luminosity regimes of the $\Gamma - L_X$ relation. In the first regime that covers the luminosity

range of $L_{2-10} \sim 10^{43} - 2 \times 10^{45}$ erg s $^{-1}$ we find a linear relation between Γ and $\log L_{2-10}$. In the second regime, where $L_{2-10} \gtrsim 2 \times 10^{45}$ erg s $^{-1}$, we confirm the finding of Dai et al. (2004) that Γ decreases with L_{2-10} . Specifically, for the 16 sources with $L_{2-10} \gtrsim 2 \times 10^{45}$ erg s $^{-1}$, we found Γ and L_X to be anti-correlated with a Spearman correlation coefficient of $r_s \sim -0.50$ that is significant at the 95.4% confidence level. We also found that for the 84 X-ray luminous sources with L_{2-10} in the range of $10^{43} - 8 \times 10^{45}$ erg s $^{-1}$ Γ and z are not correlated with a Spearman correlation coefficient of ~ 0.09 that is significant at the $\lesssim 60\%$ confidence level.

5.2.8. Physical Interpretation of the $\Gamma - L_X$ Relation and its Possible Evolution

AGN X-ray variability studies have proven very useful for improving our understanding of the physical structures that produce AGN X-ray spectra. Several variability studies of individual AGN have found a positive correlation between Γ and the X-ray luminosity, (e.g., Magdziarz et al. 1998; Zdziarski et al. 2003). However, the slope of the $\Gamma - L_X$ correlation found in the studies of individual AGNs appears to be significantly steeper than the Γ versus L_X slope found in our current study. For example, Zdziarski et al. (2003) report that a change in L_X by a factor of 10 results in an increase in Γ of ~ 0.6 . For a similar change in L_X , we find an increase in Γ of $\sim 0.2-0.3$ (see Table 5).

To explain the $\Gamma - L_X$ correlation, we present two steady state corona models proposed by Haardt et al. (1997) and Merloni & Fabian (2001). These coronal models were originally aimed to explain various X-ray variability observations of individual objects and therefore assume a constant black-hole mass. We also introduce a third model (Merloni & Fabian 2002) focused on the relative strength of the corona emission and the accretion rate. The main goal for using this model is to provide a possible connection for the results obtained in our work with the $\Gamma - L_{\text{bol}}/L_{\text{Edd}}$ correlations found by Wang et al. (2004) and Shemmer et al. (2006). At the end of this section we also comment on how the $\Gamma - L_X$ correlation depends on the optical depth of the hot corona and its evolution with z .

The first model posits that the inner accretion disk is sandwiched by a hot, tenuous and possibly patchy corona (Haardt et al. 1997). The corona is coupled to a cooler optically-thick layer (accretion disk), which provides the seed soft photons that cool the hot layer via inverse Compton scattering. The spectrum of the scattered photons is in general well fitted by a power-law and accounts for a large fraction of the observed X-ray emission in AGNs. This model predicts that Γ increases with the optical depth of the corona τ and it decreases with the temperature of the corona. Moreover, if the corona is dominated by e^\pm pairs, the optical depth of the hot phase is determined by the compactness ℓ alone⁹, where ℓ is defined as:

$$\ell \equiv \frac{\sigma_T}{m_e c^3} \frac{L_X}{R} \approx 10^4 \frac{\mathcal{L}}{r} \quad (1)$$

Here \mathcal{L} is the luminosity of the corona in Eddington

⁹ e^\pm pair production becomes important for $\ell \gtrsim 10$ (e.g., see page 51 of Peterson 1997)

units, and r is its size in units of Schwarzschild radii. For the case of a pair-dominated corona this first model predicts that Γ will increase with L_X . In particular, a change in L_X of a factor of 10 is predicted to produce a $\Delta\Gamma \sim 0.2$. This predicted variation is consistent with that detected in our sample but slightly lower than that observed in variability studies of individual AGNs. When $\mathcal{L} \gtrsim 0.1 r$ ($\ell \gtrsim 1000$) the model indicates that τ saturates and does not increase beyond that luminosity (Haardt & Maraschi 1993). The first model therefore predicts a flattening of the $\Gamma - L_X$ relation for bright sources as can be seen in Figure 17.

The second model originally proposed by Merloni & Fabian (2001) assumes a static patchy corona and is often referred to as the “thundercloud” model. The X-ray spectrum in this model is produced by thermal Comptonization in spherical regions that are raised above the disc at a given height due to magnetic flares in active regions of the corona. The thundercloud model predicts a $\Gamma - L_X$ correlation that is consistent with the one we detect for high-redshift radio-quiet AGNs in the case where the luminosity of an active region increases with its increasing size at a given height. Larger active regions tend to be more luminous, cooler and produce softer spectra (i.e., Γ increases). If the size of the active region gets too large, then a saturation point is reached and the $\Gamma - L_X$ relation becomes flat for luminous sources in agreement with the combined data sample (Figure 17). The luminosity of an active region is assumed to scale with its size r via the relation $L(r) \propto r^D$, where D is a free parameter in the model which may be related to the internal structure of the region and/or radial dependence of the energy generation in the accretion disk. Any change in D will directly affect the slope of the $\Gamma - L_X$ relation, making this model more flexible to explain both our $\Gamma - L_X$ correlation in high redshift AGNs and those found in variability studies of individual AGN (Zdziarski et al. 2003).

Under the assumption that the correlation is produced by sources of similar black-hole masses, it seems natural that changes in X-ray luminosity may result from changes in the Eddington ratio $\epsilon \sim 0.1\dot{m}$, where \dot{m} is the accretion rate in units of $\dot{M}_{\text{Edd}} = \frac{L_{\text{Edd}}}{c^2}$. Specifically, assuming L_X increases with L_{bol} (see equation 21 of Marconi et al. 2004) and since $L_{\text{bol}} = \epsilon L_{\text{Edd}}$ we expect, for sources with similar mass, an increase in ϵ to result in an increase in L_X . A more detailed analysis is provided in Merloni & Fabian (2002) in the case of a coronal-outflow dominated accretion disk model. Under the assumption that the total power released from the accretion disk-corona system is $L_{\text{bol}} \equiv \epsilon L_{\text{Edd}}$, a fraction f will be released in the corona $L_X \approx f \cdot L_{\text{bol}}$. Assuming that magnetic turbulence is the main source of angular momentum transport, Merloni & Fabian (2002) concluded that the relationship between f and ϵ can be approximately modeled as a power-law $f \propto \epsilon^{-\delta}$ with $\delta \sim 0.4$. This relation is mostly independent of the mass of the black hole M_{BH} (Wang et al. 2004). Assuming that M_{BH} is kept constant then $L_X \propto \epsilon^{1-\delta}$, and therefore L_X increases with ϵ . Using these relations in combination with a steady corona model like the ones already described in this section, while assuming that τ in-

creases with ϵ , Merloni & Fabian (2002) concluded that the corona gets cooler and Γ increases with ϵ . This could give a plausible explanation for the correlation between $\Gamma - L_{\text{bol}}/L_{\text{Edd}}$ found by Shemmer et al. (2006). Based on the above, and assuming similar black-hole masses, variations in the Eddington ratio could also explain the correlation found in our work since the coronal-outflow dominated accretion disk model predicts that Γ increases with L_X .

An alternative explanation is that the $\Gamma - L_X$ correlation is driven by variations in the black-hole masses of the sources and ϵ is constant, which is in agreement with the predictions of semi-analytic models by Kauffmann & Haehnelt (2000). It is possible that the correlation could be produced in this case if the optical depth of the corona τ increases with the mass of the black hole M_{BH} . This is equivalent to assuming that ℓ increases with M_{BH} in the model of Haardt et al. (1997) for an e^\pm dominated corona. Since $\mathcal{L} \propto M_{\text{BH}}$, the previous assumption is valid if we assume that the size of the corona is kept approximately constant as M_{BH} increases (see equation (1)). Under this assumption, both steady corona models (Haardt et al. 1997; Merloni & Fabian 2001) analyzed here will reproduce the $\Gamma - L_X$ relation.

The possible evolution of the slope and offset of the $\Gamma - L_X$ correlation found in this study of RQ AGNs can be explained by an evolution of the properties of the hot corona. Specifically, the slope of the $\Gamma - L_X$ correlation depends on the optical depth and compactness parameter of the corona in the model of Haardt et al. (1997) and the optical depth of the active regions in the thundercloud model by Merloni & Fabian (2001). If AGNs within a certain redshift range contain hot coronae of similar properties we expect them to show a significant correlation between Γ and L_X in this redshift range. One explanation of the possible evolution of the slope and offset of the $\Gamma - L_X$ correlation is that the mean properties of the hot coronae of AGN evolve resulting in a detectable change in the slope and offset of the $\Gamma - L_X$ correlation between AGNs at $z \sim 2.2$ and $z \sim 0.7$. One possible explanation for the slight decrease in the strength of the Γ and L_X correlation in the second redshift bin is that this redshift interval is comprised of AGNs having a large range of coronal properties leading to a weaker correlation between Γ and L_X . We note that the possible decrease in the significance of the Γ and L_X correlation in the second redshift bin needs to be confirmed with a larger sample of RQ AGN.

6. CONCLUSIONS

In this paper we have selected a sample of radio-quiet AGNs (173) from the CDF surveys with moderate-to-high S/N, and have found strong evidence of a correlation between the X-ray spectral parameters Γ and L_X . We found that the slope and offset of a linear fit to the $\Gamma - L_X$ correlation possibly evolves for sources with $z \gtrsim 0.1$. Analyzing this relation in three different redshift bins that contain a similar number of sources (~ 50) we conclude that this correlation is highly significant in two redshift bins, $0.3 \lesssim z \lesssim 0.96$, and $1.5 \lesssim z \lesssim 3.3$ and slightly less significant in the redshift bin $0.96 \lesssim z \lesssim 1.5$. We note that the possible weakness of this correlation for sources with $0.96 \lesssim z \lesssim 1.5$ appears to be driven by the absorbed sources in this redshift range. The $\Gamma - L_X$

correlations in $0.3 \lesssim z \lesssim 0.96$ and $1.5 \lesssim z \lesssim 3.3$ are significant at the $>99.9\%$ confidence level for fits performed in the 0.5–8 keV observed-frame and at the $>99.5\%$ confidence level in the 2–10 keV rest-frame.

The fact that this correlation is also present when we estimate the luminosities in the 2–10 keV rest-frame, and also holds for sources with low column densities, suggests that this correlation is not artificially driven by any unmodeled complexity in the intrinsic absorption (N_{H}). We performed several tests to investigate whether the $\Gamma - L_{\text{X}}$ correlation found in this study is produced by a change with luminosity of the Compton-reflection component. We found that the strengths and slopes of the $\Gamma - L_{\text{X}}$ correlation are similar for fits performed in the 0.5–8 keV observed-frame and 2–10 keV rest-frame bands. Our analysis indicates that the strengths and slopes would be significantly different if the correlation was driven by a Compton-reflection component. The difference between the observed weighted mean values of Γ obtained from fits performed in the 0.5–8 keV observed-frame and 2–10 keV rest-frame bands is less than 0.03. Our simulations indicate that if an un-modeled Compton-reflection component was producing the observed correlation a difference of Γ of about 0.2 would be expected. We conclude that a Compton-reflection component is unlikely driving the $\Gamma - L_{\text{X}}$ correlation found in this study.

This correlation applies to sources with two different luminosity populations; one with $\log L_{2-10} \sim 43.1 \pm 0.5$ ($0.3 \lesssim z \lesssim 0.96$), and the other with $\log L_{2-10} \sim 44.1 \pm 0.4$ ($1.5 \lesssim z \lesssim 3.3$) (see Figure 9), indicating different populations of AGNs. The $\Gamma - L_{\text{X}}$ relation results in a softening of the X-ray spectra as the luminosity of the AGNs increases.

The $\Gamma - L_{\text{X}}$ correlation found in the redshift range of $1.5 \lesssim z \lesssim 3.3$ is of special interest because it confirms a previous independent study of RQQ at $z \gtrsim 1.5$ (Dai et al. 2004). Combining data from Dai et al. (2004) and other surveys (Vignali et al. 1999; George et al. 2000; Reeves & Turner 2000; Page et al. 2003), cited in Dai et al. (2004), we find that the $\Gamma - L_{\text{X}}$ correlation becomes even more significant in the luminosity range of $L_{2-10} \sim 10^{43} - 8 \times 10^{45} \text{ erg s}^{-1}$ with a Spearman correlation coefficient of $r_S \sim 0.6$ significant at the $>99.9\%$ confidence level (null hypothesis probability $\sim 1.6 \times 10^{-9}$).

We presented two steady-corona models (Haardt et al. 1997; Merloni & Fabian 2001) that can explain both the $\Gamma - L_{\text{X}}$ correlation found in this work and the saturation observed in the L_{2-10} vs. Γ relation using the surveys analyzed in §5.2.7. Based on these models, we proposed two different interpretations to explain the $\Gamma - L_{\text{X}}$ correlation and its possible evolution with z . The first interpretation posits that this relation is driven by changes in the Eddington ratio ($\epsilon = L_{\text{bol}}/L_{\text{edd}}$) for a population of AGNs of similar mass. The second interpretation posits that the $\Gamma - L_{\text{X}}$ relation is driven by changes in the mass of the AGNs. The present analysis does not allow us to infer which of these two scenarios is primarily responsible for driving the $\Gamma - L_{\text{X}}$ correlation; however, future measurements of the black-hole masses for several AGNs in our sample will allow us to resolve this issue.

To explain the detected possible evolution of the slope and offset of the linear fit to the $\Gamma - L_{\text{X}}$ correlation we

have proposed a simple model that posits that the mean properties of the hot coronae of AGN at $z \sim 2.2$ differ significantly from those of AGN at $z \sim 0.7$. This model also assumes that within each redshift bin the optical depths of the hot coronae of the AGNs are similar.

We note that the detected change of the $\Gamma - L_{\text{X}}$ correlation found in our study applies to RQ AGNs detected in the CDFs, which are two representative and normal fields. Further X-ray spectral studies of deep *Chandra* fields will test if the detected change of the $\Gamma - L_{\text{X}}$ correlation also applies to wider fields of view. Expanding the sample will also test the correlation in narrower redshift bands and thus better constrain the epoch at which possible changes in the average emission properties of AGNs occurred.

We would like to thank Michael Eracleous for helpful discussions regarding the interpretations of our results, and Ohad Shemmer for reviewing the paper and providing useful comments and suggestions. We also wish to thank Eric Feigelson and Aaron Steffen for helpful discussions related to several of the statistical tests implemented in this work. We acknowledge financial support by NASA grant NAS8-03060. WNB acknowledges financial support from NASA LTSA grant NAG5-13035.

REFERENCES

- Akylas, A., Georgantopoulos, I., Georgakakis, A., Kitsionas, S., & Hatziminaoglou, E. 2006, *A&A*, 459, 693.
- Alexander, D.M., Bauer, F.E., Brandt, W.N., Schneider, A.E., Hornschemeier, A.E., Vignali, C., Barger, A.J., Broos, P.S., Cowie, L.L., Garmire, G.P., Townsley, L.K., Bautz, M.W., Chartas, & Sargent, W.L.W. 2003, *AJ*, 126, 539.
- Alexander, D. M., Bauer, F. E., Chapman, S. C., Smail, I., Blain, A. W., Brandt, W. N., & Ivison, R. J. 2005, *ApJ*, 632, 736.
- Afonso J., Mobasher, B., Koekemoer, A., Norris, R.P., & Cram, L. 2006, *AJ*, 131, 1216.
- Arnouts, S., Vandame, B., Benoist, C., Groenewegen, M. A. T., da Costa, L., Schirmer, M., Mignoli, R. P., Slijkhuis, R., Hatziminaoglou, E., Hook, R., Madejsky, R., Rit, C., & Wicenec, A. 2001, *A&A*, 379, 740.
- Barger, A.J., Cowie, L.L., Capak, O., Alexander, D.M., Bauer, F.M., Fernandez, E., Brandt, W.N., Garmire, G.P., & Hornschemeier, A.E. 2003, *AJ*, 126, 632.
- Bauer, F.E., Alexander, D.M., Brandt, W.N., Schneider, D.P., Treister, E., Hornschemeier, A.E., & Garmire, G.P. 2004a, *AJ*, 128, 2048.
- Bauer, F. E., Vignali, C., Alexander, D. M., Brandt, W. N., Garmire, G. P., Hornschemeier, A. E., Broos, P. S., Townsley, L. K., Schneider, D. P. 2004b, *Adv. Space Res.*, 34, 2555.
- Bauer, F. E., ... in prep.
- Benitez, N., 2000, *ApJ*, 536, 571.
- Bianchi, S., Guainazzi, M., Matt, G., & Fonseca Bonilla, N. 2007, *arXiv:astro-ph/0703433*
- Boyle, B.J., Fong, R., & Shanks, T. 1987, *MNRAS*, 227, 717.
- Brandt, W.N. & Hasinger, G. 2005, *ARAA*, 43, 827.
- Broos, P., Townsley, L., Getman, K., & Bauer, F. 2005, *ACIS Extract, An ACIS Point Source Extraction Package*, Pennsylvania State University, http://www.astro.psu.edu/xray/docs/TARA/ae_users_guide.html.
- Cash, W. 1979, *ApJ*, 228, 939.
- Chiang, J., Reynolds, C. S., Blaes, O. M., Nowak, M. A., Murray, N., Madejski, G., Marshall, H. L., & Magdziarz, P. 2000, *ApJ*, 528, 292.
- Cohen, J.G., Hogg, D.W., Blandford, R., Cowie, L.L., Hu, E., Songaila, A., Shopbell, P., Richberg, K. 2000, *ApJ*, 538, 29.
- Colbert, J.W., Teplitz, H.I., Yan, L., Malkan, M.A., & McCarthy, P.J., 2005, *ApJ*, 621, 587.
- Cowie, L.L., Barger, A.J., Hu, E.M., Capak, P., & Songaila, A. 2004, *AJ*, 127, 3137.
- Croom, Scott M., Warren, S. J., Glazebrook, K. 2001, *MNRAS*, 328, 150.
- Dai, X., Chartas, G., Eracleous, M., & Garmire, G.P. 2004, *ApJ*, 605, 45.
- Dwelly, T., & Page, M.J., 2006, *MNRAS*, 372, 1755.
- George, I.M & Fabian, A.C. 1991, *MNRAS*, 249, 352.
- George, I.M., Turner, T.J., Yaqoob, T., Netzer, H., Laor, A., Muchotzki, R.F., Nandra, K., & Takahashi, T. 2000, *ApJ*, 531, 52.
- Ghisellini, G., Haardt, F., & Matt, G. 1994, *MNRAS*, 267, 743.
- Giacconi, R., Zirm, A., Wang, J., Rosati, P., Nonino, M., Tozzi, P., Gilli, R., Mainieri, V., Hasinger, G., Kewley, L., Bergeron, J., Borgani, S., Gilmozzi, R., Grogin, N., Koekemoer, A., Schreier, E., Zheng, W., & Collin, N. 2002, *ApJS*, 139, 369.
- Gialalisco, M., Ferguson, H.C., Koekemoer, A.M., Dickinson, M., Alexander, D.M., Bauer, F. E., Bergeron, J., Biagetti, C., Brandt, W. N., Casertano, S., Cesarsky, C., Chatzichristou, E., Conselice, C., Cristiani, S., Da Costa, L., Dahlen, T., de Mello, D., Eisenhardt, P., Erben, T., Fall, S. M., Fassnacht, C., Fosbury, R., Fruchter, A., Gardner, J. P., Grogin, N., Hook, R. N., Hornschemeier, A. E., Idzi, R., Jogle, S., Kretchner, C., Laidler, V., Lee, K. S., Livio, M., Lucas, R., Madau, P., Mobasher, B., Moustakas, L.A., Nonino, M., Padovani, P., Papovich, C., Park, Y., Ravindranath, S., Renzini, A., Richardson, M., Riess, A., Rosati, P., Schirmer, M., Schreier, E., Somerville, R.S., Spinrad, H., Stern, D., Stiavelli, M., Strolger, L., Urry, C.M., Vandame, B., Williams, R., & Wolf, C. 2004, *ApJ*, 600, 93.
- Hasinger, G., Miyaji, T., & Schmidt, M. 2005, *A&A*, 441, 417.
- Haardt, F., & Maraschi, L. 1993 *ApJ*, 413, 507.
- Haardt, F., Maraschi, L., & Ghisellini, G. 1997 *ApJ*, 476, 620.
- Hopkins, P.F., Hernquist, L., Cox, T.J., Di Matteo, T., Martini, P., Robertson, B., & Springel, V. 2005 *ApJ*, 632, 81.
- Iwasawa, K., Taniguchi, Yoshiaki 1993, *ApJ*, 413, 15L
- Isobe, T., Feigelson, E.D., Nelson, P.I., 1986, *ApJ*, 306, 490.
- Jiang, P., Wang, J. X., & Wang, T. G. 2006, *ApJ*, 644, 725.
- Kauffmann, G., & Haehnelt, M. 2000, *MNRAS*, 311, 576.
- Konigl, A., & Kartje, J. F. 1994, *ApJ*, 434, 446.
- La Franca, F., Fiore, F., Comastri, A., Perola, G. C., Sacchi, N., Brusa, M., Cocchia, F., Feruglio, C., Matt, G., Vignali, C., Carangelo, N., Ciliegi, P., Lamastra, A., Maiolino, R., Mignoli, M., Molendi, S., Puccetti, S. 2005, *ApJ*, 635, 864L.
- Le Fèvre, O., Vettolani, G., Garilli, B., Tresse, L., Bottini, D., Le Brun, V., Maccagni, D., Picat, J. P., Scaramella, R., Scodreggio, M., Zanichelli, A., Adami, C., Arnaboldi, M., Arnouts, S., Bardelli, S., Bolzonella, M., Cappi, A., Charlot, S., Ciliegi, P., Contini, T., Foucaud, S., Franzetti, P., Gavignaud, I., Guzzo, L., Ilbert, O., Iovino, A., McCracken, H. J., Marano, B., Marinoni, C., Mathez, G., Mazure, A., Meneux, B., Merighi, R., Paltani, S., Pell, R., Pollo, A., Pozzetti, L., Radovich, M., Zamorani, G., Zucca, E., Bondi, M., Bongiorno, A., Busarello, G., Lamareille, F., Mellier, Y., Merluzzi, P., Ripepi, V., & Rizzo, D. 2005, *A&A*, 439, 845.
- Lee, J. C., Fabian, A. C., Reynolds, C. S., Brandt, W. N., Iwasawa, K. 2000, *MNRAS*, 318, 857.
- Lockman 2004, *Soft X-Ray Emission from Clusters of Galaxies and Related Phenomena*, ed. R. Lieu (Dordrecht: Kluwer), 111.
- Marconi, A., Risaliti, G., Gilli, R., Hunt, L.K., Maiolino, R., & Salvati, M., 2004, *MNRAS*, 351, 169.
- Magdziarz, P., Blaes, O.M., Zdziarski, A.A., Johnson, W.N., & Smith, D.A., 1998, *MNRAS*, 301, 179.
- Magdziarz, P., Zdziarski, A. A., 1995, *MNRAS*, 273, 837.
- Merloni, A., & Fabian, A.C., 2001, *MNRAS*, 328, 958.
- Merloni, A., & Fabian, A.C., 2002, *MNRAS*, 332, 165.
- Mobasher, B., Idzi, R., Bentez, N., Cimatti, A., Cristiani, S., Daddi, E., Dahlen, T., Dickinson, M., Erben, T., Ferguson, H. C., Gialalisco, M., Grogin, N. A., Koekemoer, A. M., Mignoli, M., Moustakas, L. A., Nonino, M., Rosati, P., Schirmer, M., Stern, D., Vanzella, E., Wolf, C., & Zamorani, G. 2004, *ApJ*, 600, 167.
- Muxlow, T.W.B., Richards, A.M.S., Garrington, S.T., Wilkinson, P.N., Anderson, B., Richards, E.A., Axon, D.J., Fomalont, E.B., Kellermann, K.I., Partridge, R.B., & Windhorst, R.A. 2005, *MNRAS*, 358, 1159.
- Nandra, K., Fabian, A. C., Brandt, W. N., Kunieda, H., Matsuoka, M., Mihara, T., Ogasaka, Y., & Terashima, Y. 1995, *MNRAS*, 276, 1.
- Nandra, K., George, I. M., Mushotzky, R. F., Turner, T. J., & Yaqoob, T. 1997 *ApJ*, 488, 91.
- Norris, R.P., Afonso, J., Appleton, P.N., Boyle, B.J., Ciliegi, P., Croom, S.M., Huynh, M.T., Jackson, C.A., Koekemoer, A.M., Lonsdale, C.J., Middelberg, E., Mobasher, B., Oliver, S.J., Polletta, M., Siana, B.D., Smail, I., & Voronkov, M.A. 2006, *AJ*, 132, 2409.
- Nousek, J.A., & Shue, D.R., 1989, *ApJ*, 342, 1207.
- Page, K.L., Turner, M.J.L., Reeves, J.N., O'Brien, P.T., & Sembay, S., 2002, *MNRAS*, 338, 1004.
- Page, K. L., O'Brien, P. T., Reeves, J. N., & Turner, M. J. L. 2004, *MNRAS*, 347, 316.
- Page, K. L., Reeves, J. N., O'Brien, P. T., Turner, M. J. L., & Worrall, D. M. 2004, *MNRAS*, 353, 133.
- Page, K. L.; Reeves, J. N.; O'Brien, P. T.; & Turner, M. J. L. 2005, *MNRAS*, 364, 195.
- Paolillo, M., Schreier, E. J., Giacconi, R., Koekemoer, A. M., Grogin, N. A., 2004, *AJ*, 611, 93.
- Peterson, B. M., 1997. *An Introduction to Active Galactic Nuclei*. Cambridge University Press.
- Reeves, J.N., Turner, M.J.L., Ohashi, T., & Kii, T. 1997, *MNRAS*, 292, 468.
- Reeves, J.N., & Turner, M.J.L. 2000, *MNRAS*, 316, 234.
- Richards, E.A., Kellermann, K.I., Fomalont, E.B., Windhorst, R.A., & Partridge, R.B. 1998, *AJ*, 116, 1039.
- Richards, E.A. 2000, *ApJ*, 533, 611.
- Schmidt, M. 1968, *AJ*, 151, 393.
- Shemmer, O., Brandt, W.N., Netzer, H., Maiolino, R., & Kaspi, S., 2006, *ApJ*, 646, L29.

- Stark et al. 1992; ApJS, 79, 77.
- Steffen, A. T., Barger, A. J., Cowie, L. L., Mushotzky, R. F., & Yang, Y. 2003, ApJL, 596, L23.
- Steidel, C.C., Adelberger, K.L., Shapley, A.E.; Pettini, M., Dickinson, M., & Giavalisco, M. 2003, ApJ, 592, 728.
- Szokoly, G.P., Bergeron, J., Hasinger, G., Lehmann, I., Kewley, L., Mainieri, V., Nonino, M., Rosati, P., Giacconi, R., Gilli, R., Gilmozzi, R., Norman, C., Romaniello, M., Schreier, E., Tozzi, P., Wang, J. X., Zheng, W., & Zirm, A. 2004, ApJS, 155, 271.
- Tozzi, P., Gilli, R., Mainieri, V., Norman, C., Risaliti, G., Rosati, P., Bergeron, J., Borgani, S., Giacconi, R., Hasinger, G., Nonino, M., Streblyanska, A., Szokoly, G., Wang, J.X., & Zheng, W. 2006, A&A, 451, 457.
- Townsley, L. K., Broos, P. S., Nousek, J. A., & Garmire, G. P. 2002, Nuclear Instruments and Methods in Physics Research A, 486, 751.
- Townsley, L. K., Feigelson, E. D., Montmerle, T., Broos, P. S., Chu, Y. H., & Garmire, G. P. 2003, ApJ, 593, 874.
- Triester, E., & Urry, C. M. 2006, ApJ652, L79-L82.
- Ueda, Y., Akiyama, M., Ohta, K., & Miyaji, T. 2003, ApJ, 598, 886.
- Vignali, C., Comastri, A., Capi, M., Palumbo, G.G.C., Matsuoka, M., & Kubo, H. 1999, ApJ, 516, 582.
- Wadadekar, Y. 2004, A&A, 416, 35.
- Warren, S.J., Hewett, P.C., & Osmer, P.S. 1994, ApJ, 421, 412.
- Wang, J., Watarai, K., & Mineshige, S., 2004, ApJ, 607, L107.
- Wirth, G.D., Willmer, C.N.A., Amico, P., Chaffee, F.H., Goodrich, R.W., Kwok, S., Lyke, J.E., Mader, J.A., Tran, H.D., Barger, A.J., Cowie, L.L., Capak, P.C., Alison L., Cooper, M.C., Conrad, A., Davis, M., Faber, S.M., Hu, E.M., Koo, David C., Le Mignant, D., Newman, J.A., & Songaila, A., 2004, AJ, 127, 3121.
- Wolf, C., Meisenheimer, K., Kleinheinrich, M., Borch, A., Dye, S., Gray, M., Wisotzki, L., Bell, E. F., Rix, H.-W., Cimatti, A., Hasinger, G., & Szokoly, G. 2004, A&A, 421, 913.
- Vanzella, E., Cristiani, S., Dickinson, M., Kuntschner, H., Nonino, M., Rettura, A., Rosati, P., Vernet, J., Cesarsky, C., Ferguson, H. C., Fosbury, R. A. E., Giavalisco, M., Grazian, A., Haase, J., Moustakas, L. A., Popesso, P., Renzini, A., & Stern, D. 2006, A&A, 454, 423.
- Zdziarski, A.A., Lubinski, P., Gilfanov, M., & Revnivtsev, M., 2003, MNRAS, 342, 355.
- Zheng, W., Mikles, V.J., Mainieri, V., Hasinger, G., Rosati, P., Wolf, C., Norman, C., Szokoli, G., Gilli, R., & Tozzi, P. 2004, ApJS, 155, 73.